Potential non-linearities in the high latitude circulation and ozone response to Stratospheric Aerosol Injection

Ewa M. Bednarz[1], Daniele Visioni[2], Amy Hawes Butler[3], Ben Kravitz[4], Douglas G MacMartin[5], and Simone Tilmes[6]

[1]CIRES / NOAA CSL
[2]Department of Earth and Atmospheric Sciences
[3]NOAA Chemical Sciences Laboratory
[4]Indiana University
[5]Cornell University
[6]National Center for Atmospheric Research (UCAR)

June 1, 2023

Abstract

The impacts of Stratospheric Aerosol Injection (SAI) on the atmosphere and surface climate depend on when and where the sulfate aerosol precursors are injected, as well as on how much surface cooling is to be achieved. We use a set of CESM2(WACCM6) SAI simulations achieving three different levels of global mean surface cooling and demonstrate that unlike some direct surface climate impacts driven by the reflection of solar radiation by sulfate aerosols, the SAI-induced changes in the high latitude circulation and ozone are more complex and could be non-linear. This manifests in our simulations by disproportionally larger Antarctic springtime ozone loss, significantly larger intra-ensemble spread of the Arctic stratospheric jet and ozone responses, and non-linear impacts on the extratropical modes of surface climate variability under the strongest-cooling SAI scenario compared to the weakest one. These potential non-linearities may add to uncertainties in projections of regional surface impacts under SAI.

Potential non-linearities in the high latitude circulation and ozone response to Stratospheric Aerosol Injection

Ewa M. Bednarz[1,2,3], Daniele Visioni[3,4], Amy H. Butler[2], Ben Kravitz[5,6], Douglas G. MacMartin[3], Simone Tilmes[4]

1. Cooperative Institute for Research in Environmental Sciences (CIRES), University of Colorado Boulder, Boulder, CO, USA
2. NOAA Chemical Sciences Laboratory (NOAA CSL), Boulder, CO, USA
3. Sibley School of Mechanical and Aerospace Engineering, Cornell University, Ithaca, NY, USA
4. Atmospheric Chemistry Observations and Modelling (ACOM), National Center for Atmospheric Research (NCAR), Boulder, CO, USA
5. Department of Earth and Atmospheric Sciences, Indiana University, Bloomington, IN, USA
6. Atmospheric Sciences and Global Change Division, Pacific Northwest National Laboratory, Richland, WA, USA

Key points

- Impacts of Stratospheric Aerosol Injection (SAI) depend on how much surface cooling is to be achieved.

- High latitude circulation, ozone and modes of extratropical variability can vary non-linearly with the SAI-induced global surface cooling

- These potential non-linearities may add to uncertainties in projections of regional surface impacts under SAI

Abstract

The impacts of Stratospheric Aerosol Injection (SAI) on the atmosphere and surface climate depend on when and where the sulfate aerosol precursors are injected, as well as on how much surface cooling is to be achieved. We use a set of CESM2(WACCM6) SAI simulations achieving three different levels of global mean surface cooling and demonstrate that unlike some direct surface climate impacts driven by the reflection of solar radiation by sulfate aerosols, the SAI-induced changes in the high latitude circulation and ozone are more complex and could be non-linear. This manifests in our simulations by disproportionally larger Antarctic springtime ozone loss, significantly larger intra-ensemble spread of the Arctic stratospheric jet and ozone responses, and non-linear impacts on the extratropical modes of surface climate variability under the strongest-cooling SAI scenario compared to the weakest one. These potential non-linearities may add to uncertainties in projections of regional surface impacts under SAI.

Plain Language Summary

The injection of reflective aerosols, or their precursors, into the lower stratosphere (Stratospheric Aerosol Injection, SAI) has been proposed as a temporary measure to offset some of the adverse impacts of climate change whilst atmospheric concentrations of greenhouses are being stabilised and, ultimately, reduced. The impacts of SAI on the atmosphere and surface climate would depend on when and where the sulfate aerosol precursors are injected, as well as on how much surface cooling is to be achieved. Here we analyze SAI impacts on stratospheric climate and ozone in a set of Earth system model simulations under varying magnitudes of the SAI-induced global mean cooling. We demonstrate that unlike some of the direct surface climate impacts from the reflection of solar radiation by sulfate aerosols, the SAI-induced changes in stratospheric circulation, chemistry and climate are more complex, with the model simulations pointing towards more non-linear behaviour of the high latitude circulation and ozone under higher SAI scenarios.

These potential non-linearities may add to uncertainties in projections of regional surface impacts under SAI.

1. Introduction

The injection of reflective aerosols, or their precursors, into the lower stratosphere (Stratospheric Aerosol Injection, SAI) has been proposed as a temporary measure to offset some of the adverse impacts of climate change whilst atmospheric concentrations of greenhouses are being stabilised and, ultimately, reduced. Research in support of informed decision making for potential future SAI requires a detailed assessment of the effectiveness and efficiency of SAI as well as the associated side-effects. The latter include the warming in the tropical lower stratosphere from the absorption of radiation by sulfate aerosols, which can then impact the large-scale Brewer Dobson Circulation (BDC) and stratospheric polar jets, driving changes in both transport of stratospheric ozone and the mid and high latitude surface climate via stratosphere-troposphere coupling (e.g., Ferraro et al., 2015; McCusker et al., 2015; Jones et al., 2022; Banerjee et al., 2021; Bednarz et al., 2022; Tilmes et al., 2021; 2022). In addition, the activation of atmospheric halogens on aerosol surfaces can accelerate catalytic ozone depletion and, thus, slow down the ongoing recovery of stratospheric ozone layer to its pre-1980 levels (e.g. Tilmes et al., 2021; 2022).

The effectiveness of SAI in reducing surface temperatures and mitigating regional climate change will depend on where and when the aerosol precursors are injected (Visioni et al., 2023a; Bednarz et al., 2023a; 2023b; Zhang et al, 2023). In addition, the effectiveness of parallel GHG emission reductions will determine the overall magnitude of SAI needed to maintain or cool the temperatures to a desired level, and the resulting SAI impacts will thus also depend on this desired temperature target (MacMartin et al., 2022; Visioni et al., 2023b). Visioni et al., (2023b) analysed some of the surface climate responses in a set of SAI simulations using the same injection strategy (i.e. the same location of SO_2 injections) but achieving different levels of global mean surface cooling (though different total magnitudes of SAI), and showed that many of the resulting changes scale broadly linearly with the amount of SAI-induced cooling.

Though the direct radiative changes at the surface behave quasi linearly with the amount of SAI, the behaviour of the stratosphere-troposphere coupled circulation has been shown to be non-linear or regime-like in character in response to external forcings, both idealised thermal forcings and climate change (Charney and Drazin, 1961, Wang et al., 2012; Manzini et al., 2018; Walz et al., 2023), and thus harder to predict. Similarly, in the stratosphere the concentrations of chemical tracers like ozone are driven by a range of chemical and dynamical processes, the relative contribution of which could change under SAI. Here we extend the work of Visioni et al., (2023b) by analysing the impacts of SAI on stratospheric climate and ozone under varying magnitudes of global mean cooling. We demonstrate that while the tropical stratospheric changes behave largely linearly, the resulting high latitude dynamical responses to SAI are more complex and could vary non-linearly with increasing magnitudes of SAI. These in turn could lead to non-linear impacts on high-latitude climate and ozone that may add to uncertainties in projections of some regional surface impacts under SAI.

2. Methods

We use the CESM2(WACCM6) earth system model (Gettelman et al., 2019; Danabasoglu et al., 2020) with interactive modal aerosol microphysics (MAM4, Liu et al., 2016) and interactive middle atmosphere chemistry (Davis et al., 2023). The horizontal resolution is 1.25° longitude by 0.9° latitude, with 70 vertical levels in hybrid-pressure coordinates up to ~140 km. The simulations used are introduced in MacMartin et al. (2022) and described in detail in Visioni et al. (2023b). The Coupled Model Intercomparison Project Phase 6 (CMIP6) Shared Socioeconomic Pathway SSP2-4.5 experiment is chosen as a background emission scenario. In all SAI simulations SO_2 is injected at 21.5 km at four off-equatorial latitudes – 30°S, 15°S, 15°N, 30°N – using a feedback algorithm that controls for the global mean surface temperature as well as its large scale interhemispheric and equator-to-pole gradients.

Three SAI scenarios, each consisting of three ensemble members, start in 2035 and continue until 2069 inclusive. 'SAI1.5' maintains the above three temperature objectives at the levels corresponding to 1.5°C above preindustrial conditions, with total SO_2 injection of 8.6 Tg-SO_2/yr averaged over the last 20 years of simulations. This baseline was chosen as corresponding to the 2020-2039 mean of the CESM2 SSP2-4.5 simulation ('BASE1.5'). 'SAI1.0' and 'SAI0.5' are similar to SAI1.5 but aim to achieve more surface cooling by injecting more SO_2 (17.0 and 25.6 Tg-SO_2/yr averaged over the last 20 years of simulations, respectively), with the desired global mean surface temperatures of 1.0°C and 0.5°C above preindustrial conditions, respectively; these baseline periods correspond in CESM2 to the mean over the 2008-2027 and 1993-2012 periods, respectively.

We analyse the last 20-years of the simulations (2050-2069) and compare them against the same period of the control SSP2-4.5 simulation and/or against the same BASE1.5 baseline period representative of quasi-present day conditions. This avoids complications from the different contributions of the concurrent changes in GHGs and ozone depleting substances if the SAI responses are compared against each individual baseline period instead (see Visioni et al. 2023b for more discussion on the role of the choice of baseline period).

3. Changes in tropical stratospheric climate

The introduction of sulfate aerosols into the stratosphere and the resulting scattering of a portion of coming solar radiation reduces tropical tropospheric temperatures, with the strongest reduction, by design, found in SAI0.5 and smallest in SAI1.5 (Fig. 1a). In the lower stratosphere, the absorption of the portion of the outgoing terrestrial and incoming solar radiation by sulfate increases local temperatures. The magnitude of this effect is in tight linear relationship with the global mean surface cooling in each of the SAI simulation, with R^2 = 0.95 for the goodness of fit of the individual ensemble members and R^2=1.00 for the fit to the ensemble means (Fig. 1e).

The SAI-induced lower stratospheric warming drives changes in the large-scale circulation, decelerating the shallow branch of the BDC and accelerating the deep branch (see Fig. 1b for changes in residual vertical velocities; by mass continuity, these are closely related to changes in horizontal velocities). Changes in the large-scale transport modulate stratospheric distribution of chemical tracers, most importantly ozone. In the tropics (Fig. 1d), this increases ozone in the tropical lower stratosphere (from reduced input of ozone-poor tropospheric air) and decreases ozone above it at ~30 hPa (from enhanced input of lower stratospheric air with lower ozone concentrations). Climatologically, the absorption of solar radiation by ozone constitutes the dominant source of heat in the stratosphere and, thus, any changes in its concentration act to further modulate stratospheric temperatures. A tight correlation between SAI-induced changes in tropical temperatures, ozone and transport was shown to hold also in a multi-model context (Bednarz et al., 2023a). In the extratropics, SAI-induced strengthening of the BDC enhances ozone transport from its tropical photochemical production region to higher latitudes, thereby increasing total column levels in the mid and high latitudes (See Section 5). Finally, the SAI-induced warming around the cold point tropical tropopause allows more water vapour to enter the stratosphere (Fig. 1c), and this acts to offset some of the direct surface cooling as water vapour traps a portion of the outgoing terrestrial radiation (Bednarz et al., 2023b). Increased stratospheric water vapour also modulates the rates of chemical ozone loss, as well as provides additional stratospheric cooling.

Overall, the magnitudes of these responses scale linearly with increasing magnitude of SAI. Whilst a strong linear relationship was found for the magnitudes of lower stratospheric warming (Fig. 1e) and BDC changes (Fig. 1f), some deviations from a linear relationship begin to emerge for changes in lower stratospheric water vapour (Fig. 1g) and ozone (Fig. 1h) under the strongest SAI scenario. The latter may reflect certain nonlinearities in aerosol microphysics under high inject rates (Visioni et al., 2023b) or a contribution of the apparent non-linearities at higher latitudes (Sections 4 and 5).

4. High latitude dynamical response

4.1. Stratosphere

The enhancement of the meridional temperature gradients as the result of SAI-induced warming in the tropical lower stratosphere drives strengthening of the stratospheric jets in both hemispheres, and the magnitude of the response increases with the magnitude of SO_2 injection (Fig. 2a-c). The degree of linearly of this response with respect to the amount of global mean surface cooling depends on the season under analysis.

In the Southern Hemisphere (SH) during austral winter (Fig. 2e), where the very strong climatological jet prohibits much planetary wave propagation and, thus, any changes are mainly radiatively driven via the thermal wind relationship, a strong linear relationship (R^2=0.94 for the fit to the ensemble means of SAI1.5, SAI1.0 and SAI0.5) is found between the magnitude of the SH jet strengthening and the global mean surface cooling. However, in spring (SON, Fig. 2g), when interactions with both planetary waves and with the SAI-induced ozone depletion within the polar vortex (Section 5) can occur, a more non-linear relationship emerges: the jet strengthening in the largest SAI scenario (SAI0.5) is disproportionally larger than that inferred for SAI1.0 and SAI1.5 (9 m/s, 4 m/s and 2 m/s, respectively). For the Northern Hemisphere (NH) during winter (DJF, Fig. 2d) the apparent non-linearity is even stronger: the NH jet strengthening simulated in SAI0.5 is also disproportionally larger than that in SAI1.0 and SAI1.5 (8 m/s, 4 m/s and 3 m/s, respectively), and is also characterised by a much larger spread in the zonal wind responses simulated across the individual ensemble members (blue crosses) than it is the case for either SAI1.0 and SAI1.5.

Non-linearity of the NH polar vortex response has been previously found in response to increased CO_2 forcing (Manzini et al. 2018) and to idealized heating in a dry dynamical model (Wang et al. 2012, Walz et al. 2023), and may be related to either differences in tropospheric wave forcing that arise from non-linear changes in sea ice (Kretschmer et al., 2020) or sea surface temperatures, or to regime-like behaviour in the stratospheric planetary wave guide (Walz et al. 2022).

4.2. Northern Hemisphere troposphere

Through wave-mean flow interactions, extratropical stratospheric wind changes can propagate down to the troposphere and affect surface climate (e.g. Baldwin and Dunkerton, 2001; Thompson and Wallace 2000); in the NH this coupling maximises in winter. In the absence of SAI for the SSP2-4.5 scenario, increasing tropospheric temperatures in CESM2(WACCM6) cause strengthening of zonal winds in the subtropics and weakening of zonal winds in the Arctic region (Figure S3). Thus, a comparison of SAI against SSP2-4.5 for the same future time period reflects in part the response to climate change itself (Fig. S4). In order to better isolate the influence of SAI-induced changes in the stratosphere, Figure 3 shows the tropospheric SAI responses compared to the BASE1.5 period (i.e. present day) instead.

We find that the NH stratospheric westerly changes compared the present-day period only propagate down to the troposphere under the strongest SAI scenario (SAI0.5), Fig. 3a-c. The surface response in NH winter manifests as the pattern of sea-level pressure changes projecting on the positive phase of the North Atlantic

Oscillation (NAO) (Fig. 3d-f) diagnosed also from each individual ensemble member of SAI0.5 (Fig. S5 and S6). The positive NAO response drives a dynamically induced warming over northern Eurasia, which is large enough to locally offset the large-scale cooling from the reduction in the global mean surface temperatures (Fig. S6). In contrast, no significant tropospheric jet strengthening or NAO-like sea-level pressure response is found in the two smaller SAI scenarios (SAI1.0 and SAI1.5. Fig 3a-f). While the pattern of sea-level pressure changes in SAI1.0 resembles that of a positive NAO, the ensemble mean response is very weak and not statistically significant, with little agreement between the responses simulated across the individual ensemble members (Fig. S5 and S6).

The strength of the stratosphere-troposphere coupling can be assessed by correlating the changes in the NH stratospheric jet with the NAO index for each of the ensemble members and scenarios. Following our earlier work (Bednarz et al., 2023a) we calculate the model NAO index as the difference in sea-level pressure between the Atlantic mid-latitudes (280°E-360°E, 30°N-60°N) and the Arctic polar cap (70°N-90°N, all longitudes). Over the 20-year mean period analysed here, we find a strong relationship between the strength of the stratospheric winds and surface NAO responses for the three ensemble members of the strongest SAI scenario (SAI0.5), with stronger stratospheric westerly anomalies being associated with more positive NAO values (blue points in Fig. 3g). In contrast, no such relationship can be inferred for the responses in the individual ensemble members of the two smaller SAI scenarios (SAI1.0 and SAI1.5). An analysis of temporal evolution of the responses reveals that the apparent non-linearity emerges toward the end of the simulations (Fig. S8), where the injection rates are highest.

Such apparent nonlinearity in the NH surface responses may result from the non-linearity in the stratospheric jet response itself (Section 4.1), or from non-linearities in the tropospheric circulation or sea ice and sea surface temperatures that either discourage or promote the canonical downward coupling from the stratosphere on the NAO (Kolstad et al., 2022). Another possibility is that the enhanced stratosphere-troposphere coupling under the largest SAI scenario arises because the response is only for that case strong enough to emerge from the background natural variability, which is particularly high in the NH winter (e.g. Bittner et al., 2016; DallaSanta and Polvani, 2022).

4.3. Southern Hemisphere troposphere

Anomalies in the SH stratospheric jet can also propagate down to the troposphere and affect the SH surface climate; such stratospheric influence tends to maximise in austral spring and summer (SON and DJF). We find that the SAI-induced westerly stratospheric anomalies do not propagate down to the surface in any of the SAI simulations (Fig. 3h-j). This is the case even for the strongest SAI0.5 scenario (Fig. 3j) that shows disproportionally larger stratospheric jet perturbation in spring than the smaller SAI1.0 and SAI1.5. We would expect a strengthened SH stratospheric jet in austral spring to lead to a later than average seasonal transition of the polar vortex and an associated shift towards the positive phase of the Southern Annular Mode (SAM) in austral summer (e.g. Thompson et al., 2005). Instead, all SAI scenarios give rise to a pattern of sea-level pressure changes projecting onto the negative phase of SAM, inferred both from DJF (Fig. 3h-j) and yearly mean (Fig. S9) data, with no clear linear relationship between the strength of the SAM-like sea-level pressure pattern and the SAI magnitude. This suggests that factors other than the magnitude of the injection, especially the meridional distribution of sulfate in the stratosphere (e.g. Bednarz et al., 2022, GRL), are more important in determining the SH high latitude tropospheric and surface response to SAI.

5. Impacts on Arctic and Antarctic ozone

5.1 Antarctic ozone

In austral spring, the SH high latitude ozone columns decrease under all three SAI scenarios compared to the same period of SSP2-4.5 because of the enhancement of heterogeneous halogen activation on sulfate and the resulting catalytic stratospheric ozone depletion inside the Antarctic polar vortex (Fig. 4a). In addition, the strengthening of the polar vortex inhibits mixing with the more ozone-rich mid-latitude air, thereby further reducing polar ozone levels. We find similar Antarctic (65°S-90°S) ozone losses of 26 DU (= 9%) and 30 DU (= 11%) for the two lower SAI scenarios, SAI1.5 and SAI1.0, respectively. In contrast, a significantly higher Antarctic ozone loss of 43 DU (= 15%) is found for the largest SAI0.5 scenario.

A tight linear relationship is found between the polar ozone column reduction and the strengthening of the Antarctic polar vortex across the simulations (Fig. 4d), and also between the ozone changes and the increased aerosol surface area densities (SAD, Fig. 4g). A stronger and colder polar vortex under more aggressive SAI scenario accelerates halogen activation on sulfate as well as delays final vortex break up and the resulting termination of the catalytic ozone loss by in-mixing of the mid-latitude NO_2-rich, air; both factors enhance Antarctic ozone loss under SAI. Conversely, enhanced ozone depletion under higher sulfate surface area densities results in dynamical impact on the polar vortex itself, cooling the polar stratosphere and strengthening the stratospheric zonal winds (e.g. Keeble et al., 2014). The strong linear relationship between these quantities under varying SAI levels demonstrates how the same processes operate under all three SAI scenarios. The cause of the apparent non-linearity and thus the significantly higher magnitude of the Antarctic springtime ozone loss in SAI0.5 compared to SAI1.0 and SAI1.5 is thus dynamical in origin, in line with the significantly larger strengthening of the polar vortex in SAI0.5 than the other two scenarios.

5.2 Arctic ozone

Unlike in the SH, the NH ozone column largely increases under SAI during boreal winter and spring (Fig. 4b-c) due to the SAI-induced changes in the BDC and the resulting ozone transport (Section 3). Owing to the Arctic vortex being climatologically weaker and more variable than its SH counterpart, the chemical impacts from the SAI-induced enhancement of the heterogenous halogen processing on the elevated SAD are generally smaller. They do however still contribute to the simulated column ozone changes, alongside dynamical impacts from the reductions in mixing under the strengthened Arctic polar vortex.

Consistently, SAI1.5 shows increased NH winter total ozone columns in the mid- and high latitudes up to ~75°N, with a small total column ozone decrease poleward. For SAI1.0, the total column ozone changes are positive everywhere and larger in magnitude than for SAI1.5; this indicates that the impact of SAI on the strength of the BDC dominates over chemically driven ozone reductions in this scenario. In spring, ozone columns increase throughout the NH in the ensemble mean for both SAI1.5 and SAI0.5, albeit with larger variability between the individual ensemble members than during winter (dashed lines in Fig. 4b-c).

An interesting picture emerges for the largest SAI0.5 scenario: whilst ozone columns increase in winter in the ensemble mean throughout the NH, the magnitude of the response is sharply reduced in the Arctic region, with substantially larger variability between the individual ensemble members. In fact, one ensemble member of SAI0.5 shows the strongest decrease in Arctic ozone at the pole from all the SAI simulations and members. The large intra-ensemble variability continues into spring, with individual members of SAI0.5 showing both the most positive and the most negative Arctic column ozone perturbations. The large springtime ozone variability extends to the mid-latitudes, as anomalies in polar ozone mix-in with the mid-latitude air following the vortex break-up. The contrastingly different ozone behaviour in SAI0.5 is concurrent with the strongest and more non-linear high latitude dynamical response identified above (Section 4.1-2). Owing to the interplay of various dynamical and chemical processes in the

Arctic, with its opposing impacts on total ozone column, the previously identified linear relationship between changes in the Antarctic ozone, polar vortex and sulfate SAD (Fig. 4d,g) is generally not found in the Arctic during winter(Fig. 5e,h). The inverse relationship between changes in polar ozone and vortex strength is only apparent under the strongest SAI0.5 scenario, facilitated by the much larger variability between the ensemble members.

Recent studies highlighted the role of dynamical and chemical ozone reductions inside the Arctic polar vortex in modulating the northern polar jet dynamics (Friedel et al., 2022a; 2022b; Kult-Herdin et al., 2023). However, it was also demonstrated that this ozone feedback, as manifested by the inverse relationship between polar ozone and jet strength, is only found under the present-day (i.e. high) levels of ozone-depleting substances where ozone variability is larger (Kult-Herdin et al., 2023). It is possible that the same occurs under SAI, i.e. the feedback from interactive ozone in our runs only starts to play a significant role in contributing to the polar vortex behaviour under the strongest SAI0.5 scenario, where the aerosol SAD and, thus, chemical ozone depletion is largest.

In spring, the inverse relationship between polar ozone and the vortex strength (Fig. 4f) or SAD (Fig. 4i) emerges for each individual SAI scenario. This indicates that the differences in springtime ozone responses across the different SAI scenario (Fig. 4c) are driven predominantly by the SAI-induced changes in the BDC, whereas the intra-ensemble spread in each scenario is associated more linearly with chemical-dynamical feedbacks.

6. Summary and discussion

The impacts of Stratospheric Aerosol Injection on the atmosphere and surface climate would depend on when and where the sulfate aerosol precursors are injected, as well as on how much surface cooling is to be achieved. Here we extend our recent work that explored the linearity of some of the direct surface climate impacts in a set of CESM2(WACCM6) SAI simulations achieving three different levels of a global mean surface cooling (Visioni et al., 2023b). We demonstrate that unlike some of the direct surface climate impacts from the reflection of solar radiation by sulfate aerosols, the SAI-induced changes in stratospheric circulation, chemistry and climate are more complex, with the model simulations pointing towards more non-linear behaviour of the high latitude circulation and ozone under higher SAI scenarios.

We find that the SAI-induced changes in the tropical stratospheric temperatures, upwelling, water vapour and ozone scale roughly linearly with the magnitude of global mean cooling in CESM2 under the multi-objective SAI strategy used. A significantly more non-linear behaviour is found for the associated extratropical stratospheric zonal wind responses, in particular in seasons when the wave-mean flow coupling plays an important role. In those cases, a disproportionally stronger westerly jet anomaly is simulated for the largest SAI scenario (SAI0.5) compared to the more modest ones. In the SH, this is associated with markedly stronger (~50%) Antarctic springtime ozone depletion in SAI0.5. In the NH, the non-linearity manifests in part as the significantly larger intra-ensemble spread of the SAI-induced changes in the stratospheric jet strength and Arctic ozone columns in SAI0.5. The scenario also gave rise to much stronger NH stratosphere-troposphere coupling, facilitating the propagation of the stratospheric westerly down to the surface in the form of the positive North Atlantic Oscillation, which was otherwise not reproduced for the two smaller SAI scenarios. Regarding impacts on the Southern Annular Mode, the analogous propagation of the SH polar vortex strengthening to the troposphere is not found under any SAI scenario; this points to other factors like the meridional distribution of sulfate in the stratosphere (and thus the location of the injection) being more important in determining the SAI impacts in the region.

The results highlight the complexity of the impacts of SAI on the stratospheric climate, high latitude circulation and stratospheric ozone, including the complex interplay of various chemical, radiative and dynamical processes. Dynamical mechanisms for abrupt regime changes driving the dynamical responses to thermal perturbations were previously found in idealised models (e.g. Wang et al., 2012; Walz et al., 2023). Whether these mechanisms apply also to more complex climate models is still not well understood, but non-linearities in the stratospheric jet response to different levels of global warming have previously been found (Manzini et al., 2018). The role of chemically driven Arctic and Antarctic ozone reductions in modulating the polar vortex behaviour has also been highlighted as a potentially important feedback mechanism that is still not sufficiently understood (Keeble et al., 2014; Friedel et al., 2022a; 2022b; Kult-Herdin et al., 2023). Here evidence of such feedback was shown to be particularly strong under the largest SAI scenario, i.e. when the higher stratospheric aerosol levels drive larger chemical ozone losses that can then module the polar vortex. Finally, though not examined in detail in this study, changes in stratospheric water vapour have also been shown to drive changes in the high latitude circulation (Maycock et al., 2013; Seabrook et al., 2023), as well as enhance catalytic ozone loss (e.g. Tilmes et al., 2021), but uncertainties remain as to the details of such responses. Since SAI-induced lower stratospheric warming also drives significant increases in stratospheric water vapour, this process constitutes an additional source of uncertainty to the overall SAI impacts in the high latitudes.

We note that our results could be model dependent. In addition, with three ensemble members per experiment, a rigorous assessment of the origin of these dynamical differences is beyond the scope of the current study. However, the apparent non-linear behaviour of the high latitude circulation and ozone response to SAI merits further assessment in a multi-model framework and with larger ensembles, as part of ongoing efforts in narrowing the uncertainties in the climate response to SAI.

Acknowledgements

We would like to acknowledge high-performance computing support from Cheyenne (https://doi.org/10.5065/D6RX99HX) provided by NCAR's Computational and Information Systems Laboratory, sponsored by the National Science Foundation. Support was provided by the NOAA cooperative agreement NA22OAR4320151, NOAA Earth's Radiative Budget initiative, Atkinson Center for a Sustainability at Cornell University, and by the National Science Foundation through agreement CBET-2038246. Support for BK was provided in part by the National Science Foundation through agreement SES-1754740 and the Indiana University Environmental Resilience Institute. The Pacific Northwest National Laboratory is operated for the US Department of Energy by Battelle Memorial Institute under contract DE-AC05-76RL01830.

Data access

Data used in this manuscript is available from doi: 10.5281/zenodo.7976364.

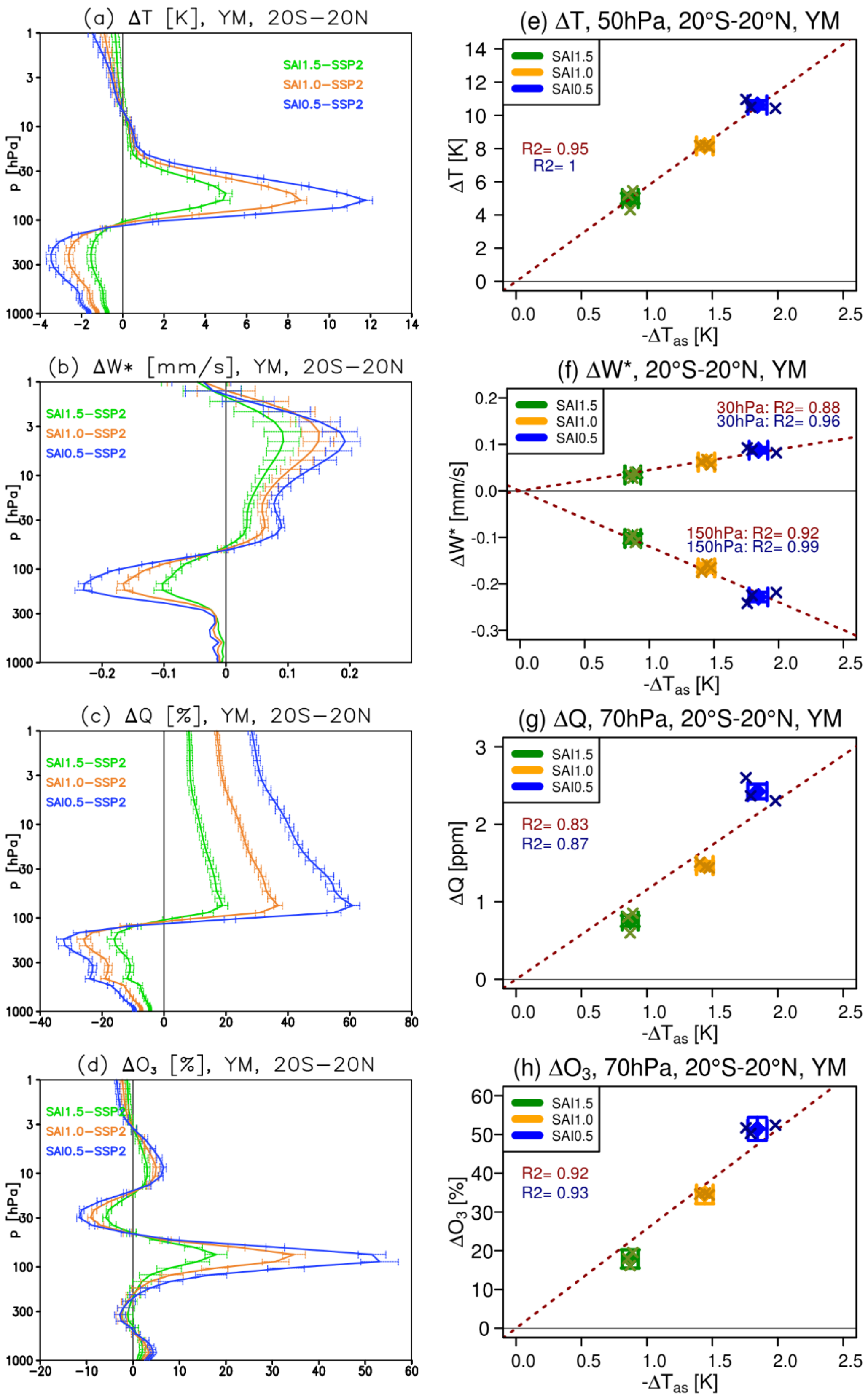

Figure 1. Left: Yearly mean changes in the ensemble mean tropical (a,e) temperatures, (b,f) TEM vertical velocity, (c,g) water vapour and (d,h) ozone for each of the SAI scenarios compared to the control SSP2-4.5 simulation for the same period (2050-2069). Error bars denote ±2 standard errors of the difference in means. Right: Scatterplot of the SAI stratospheric responses against the magnitude of the global mean surface cooling. Diamonds and whiskers indicate ensemble mean response ±2 standard error, and the crosses indicate

the responses in the individual ensemble members (compared to the ensemble mean of SSP2-4.5). Value of R^2 shown in red and blue corresponds to the value calculated for the single ensemble members and the ensemble means, respectively. See **Fig. S1** in Supplement for the analogous responses compared to the present day BASE1.5 baseline period.

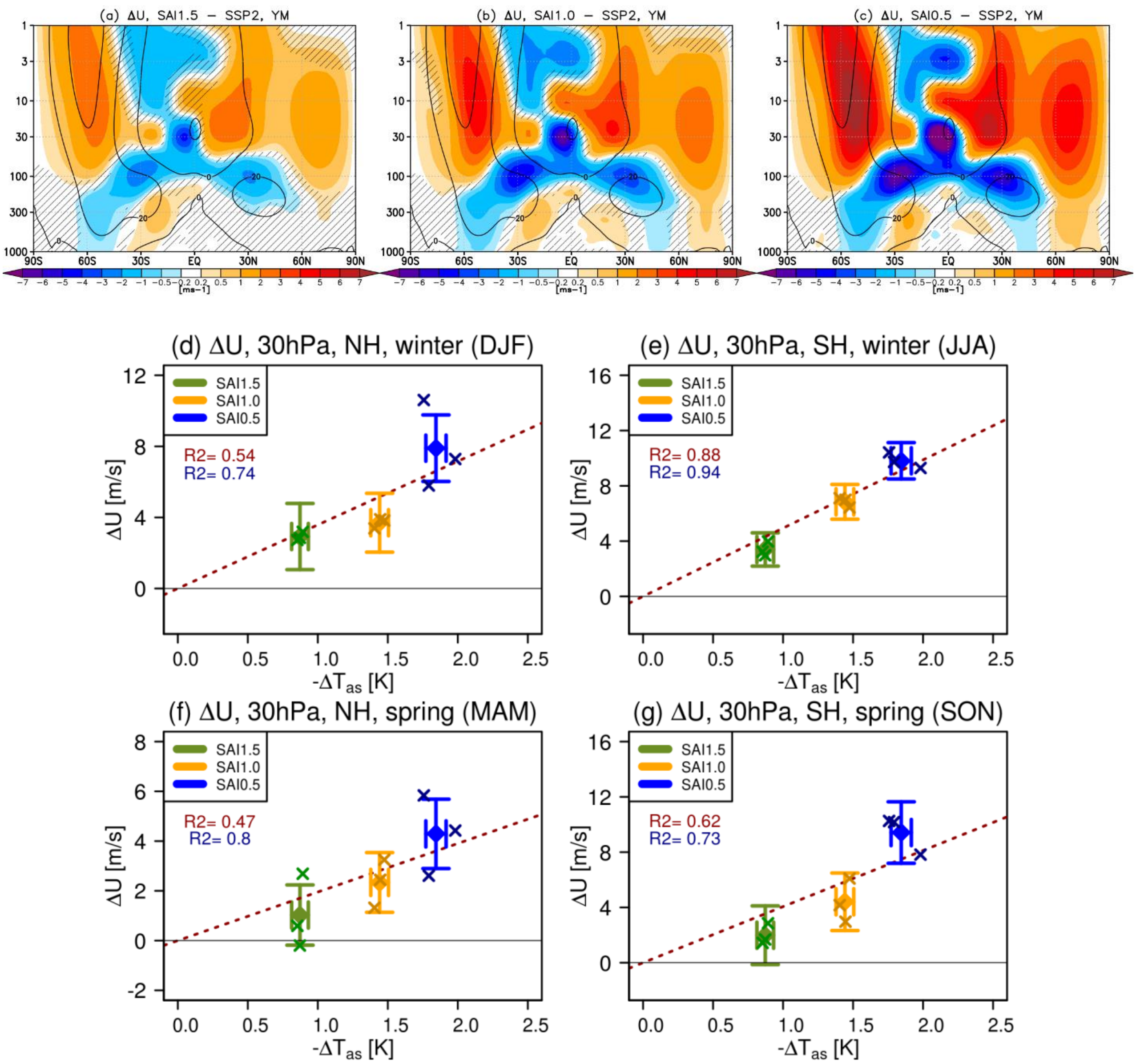

Figure 2. (a-c) Shading: yearly mean changes in zonal winds in each of the SAI simulation compared to SSP2-4.5. Contours show the values in SSP2-4.5 for reference. Hatching marks the regions where the response is not statistically significant (taken as ±2 standard error of the difference in means). (d-g) Changes in the strength of the NH (60°N, d,f) and SH (50°S, e,g) polar vortex at 30 hPa in winter (d,e) and spring (f,g) in each of the SAI scenario vs the magnitude of the global mean surface cooling compared to SSP2-4.5. Diamonds and whiskers indicate ensemble mean response ±2 standard error, and the crosses indicate the responses in the individual ensemble members (compared to the ensemble mean of SSP2-4.5). Value of R2 shown in red and blue corresponds to the value calculated for the single ensemble members and ensemble means, respectively. See **Fig. S2** in Supplement for the analogous responses compared to the present day BASE1.5 baseline period.

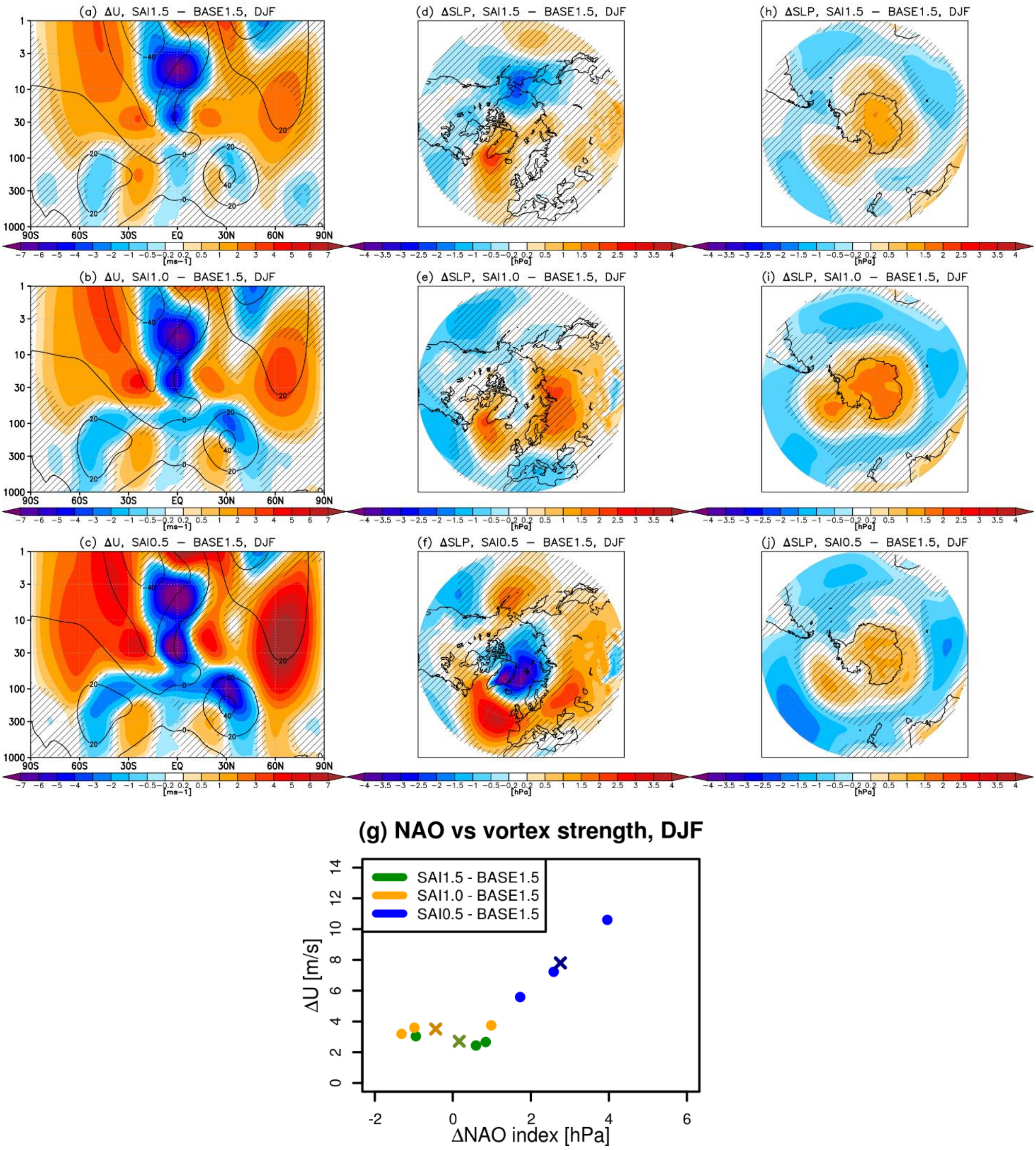

Figure 3. DJF changes in: (a-c) zonal winds, (d-f) sea-level pressures northward of 30°N, and (h-j) sea-level pressures southward of 30°S for each of the SAI scenarios compared to BASE1.5. Hatching as in Fig. 2. (g): Correlation between the DJF changes in the strength of the NH stratospheric polar vortex (60°N, 30 hPa) and the NAO sea-level pressure index for each of the SAI scenarios compared to BASE1.5. Points illustrate the responses for each of the ensemble members, and crosses the corresponding ensemble mean responses. See **Fig. S4** in Supplement for the analogous responses compared to SSP2-4.5.

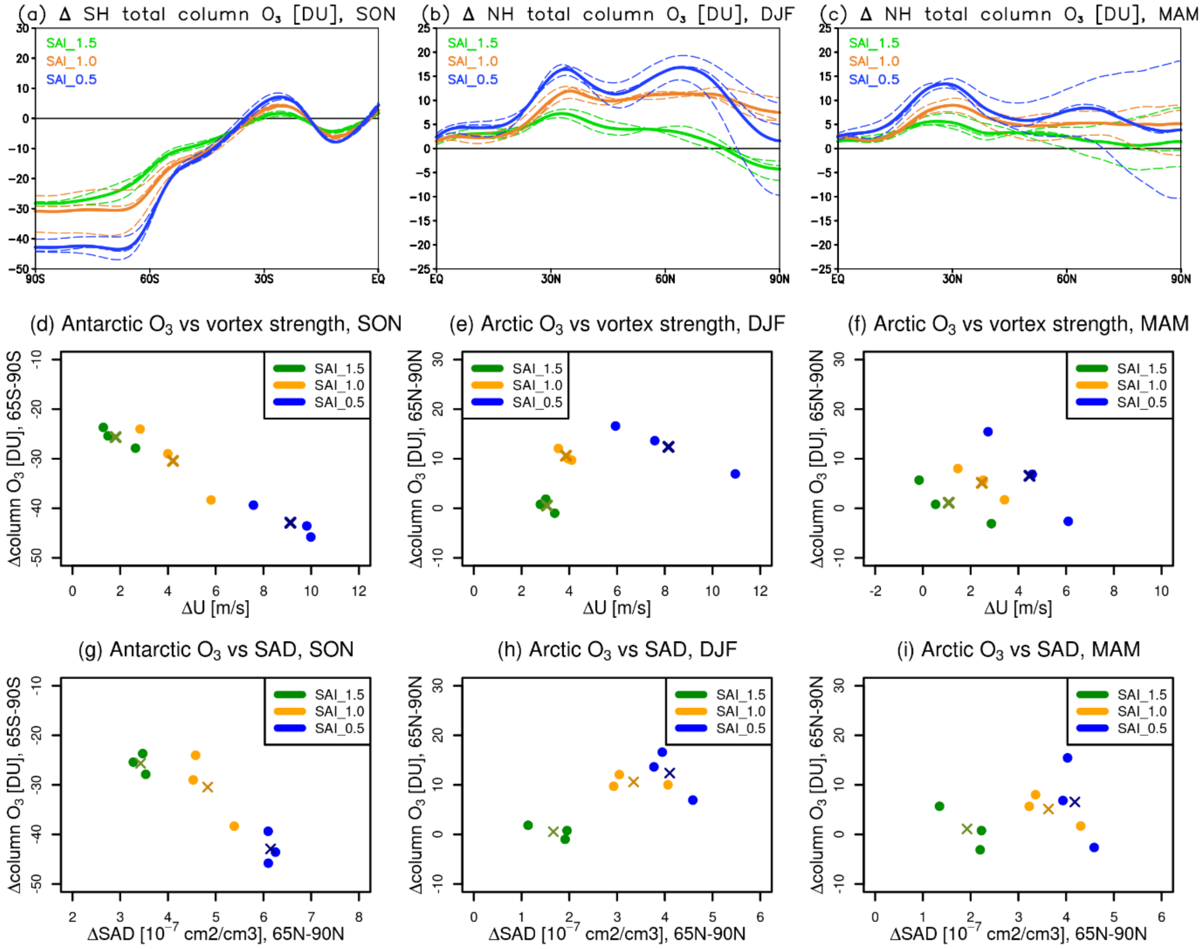

Figure 4. Impacts on the Arctic and Antarctic ozone. (a-c) Seasonal mean changes in total column ozone (left) in SON in the SH, (middle) DJF in the NH and (right) MAM in the NH for each of the SAI scenarios compared to SSP2-4.5. Thick lines denote the ensemble mean response and dashed lines the responses in each individual ensemble member (compared to the ensemble mean response in SSP2-4.5). (d-i) The correlation between seasonal mean changes in (d-f) polar ozone and stratospheric vortex strength, and between changes in (g-i) polar ozone and polar aerosol surface area density at 170 hPa. Each point represents the response in each individual ensemble member, and the cross represents the ensemble mean response.

References

Baldwin. M. P., and Dunkerton. T. J.: Stratospheric Harbingers of Anomalous Weather Regimes, Science, 294, 581-584, DOI:10.1126/science.1063315, 2001.

Banerjee, A., Butler, A. H., Polvani, L. M., Robock, A., Simpson, I. R., and Sun, L.: Robust winter warming over Eurasia under stratospheric sulfate geoengineering – the role of stratospheric dynamics, Atmos. Chem. Phys., 21, 6985–6997, https://doi.org/10.5194/acp-21-6985-2021, 2021.

Bednarz, E. M., Visioni, D., Kravitz, B., Jones, A., Haywood, J. M., Richter, J., MacMartin, D. G., and Braesicke, P.: Climate response to off-equatorial stratospheric sulfur injections in three Earth system models – Part 2: Stratospheric and free-tropospheric response, Atmos. Chem. Phys., 23, 687–709, https://doi.org/10.5194/acp-23-687-2023, 2023a.

Bednarz, E. M., Butler, A. H., Visioni, D., Zhang, Y., Kravitz, B., and MacMartin, D. G.: Injection strategy – a driver of atmospheric circulation and ozone response to stratospheric aerosol geoengineering, EGUsphere [preprint], https://doi.org/10.5194/egusphere-2023-495, 2023b.

Bednarz, E. M., Visioni , D., Richter, J. H., Butler, A. H., MacMartin , D. G.: Impact of the latitude of stratospheric aerosol injection on the Southern Annular Mode, Geophysical Research Letters, 49, e2022GL100353. https://doi.org/10.1029/2022GL100353, 2022.

Bittner, M., Schmidt, H., Timmreck, C., and Sienz, F.:Using a large ensemble of simulations to assess the Northern Hemisphere stratospheric dynamical response to tropical volcanic eruptions and its uncertainty, Geophys. Res. Lett., 43, 9324– 9332, doi:10.1002/2016GL070587, 2016.

Charney, J. G., and Drazin, P. G.: Propagation of planetary-scale disturbances from lower into upper atmosphere, Journal of Geophysical Research, 66, 83-&, 10.1029/JZ066i001p00083, 1961.

DallaSanta, K. and Polvani, L. M.: Volcanic stratospheric injections up to 160 Tg(S) yield a Eurasian winter warming indistinguishable from internal variability, Atmos. Chem. Phys., 22, 8843–8862, https://doi.org/10.5194/acp-22-8843-2022, 2022.

Danabasoglu, G., Lamarque, J.-F., Bacmeister, J., Bailey, D. A., DuVivier, A. K., Edwards, J., Emmons, L. K., Fasullo, J., Garcia, R., Gettelman, A., Hannay, C., Holland, M. M., Large, W. G., Lauritzen, P. H., Lawrence, D. M., Lenaerts, J. T. M., Lindsay, K., Lipscomb, W. H., Mills, M. J., Neale, R., Oleson, K. W., Otto-Bliesner, B., Phillips, A. S., Sacks, W., Tilmes, S., van Kampenhout, L., Vertenstein, M., Bertini, A., Dennis, J., Deser, C., Fischer, C., Fox-Kemper, B., Kay, J. E., Kinnison, D., Kushner, P. J., Larson, V. E., Long, M. C., Mickelson, S., Moore, J. K., Nienhouse, E., Polvani, L., Rasch, P. J., and Strand, W. G.: The Community Earth System Model Version 2 (CESM2), J. Adv. Model. Earth Sy., 12, e2019MS001916, https://doi.org/10.1029/2019MS001916, 2020.

Davis, N. A., Visioni, D., Garcia, R. R., Kinnison, D. E., Marsh, D. R., Mills, M. J., Richter, J. H., Tilmes, S., Bardeen, C., Gettelman, A., Glanville, A. A., MacMartin, D. G., Smith, A. K., and Vitt, F.: Climate, variability, and climate sensitivity of “Middle Atmosphere” chemistry configurations of the Community Earth System Model Version 2, Whole Atmosphere Community Climate Model Version 6 (CESM2(WACCM6)), https://doi.org/10.22541/essoar.167117634.40175082/v1, 2022.

Ferraro, A. J., Charlton-Perez, A. J., and Highwood, E. J.: Stratospheric dynamics and midlatitude jets under geoengineering with space mirrors and sulfate and titania aerosols, J. Geophys. Res.-Atmos., 120, 414–429, 2015.

Friedel, M., G. Chiodo, A. Stenke, D. Domeisen, and T. Peter: Effects of Arctic ozone on the stratospheric spring onset and its surface impact, Atmospheric Chemistry and Physics, DOI:10.5194/acp-22-13997-2022, 2022.

Friedel, M., Chiodo, G., Stenke, A. D. Domeisen, S. Fueglistaler, J. Anet, and T. Peter. Springtime arctic ozone depletion forces northern hemisphere climate anomalies. Nat. Geosci. 15, 541–547, https://doi.org/10.1038/s41561-022-00974-7, 2022.

Gettelman, A., Mills, M. J., Kinnison, D. E., Garcia, R. R., Smith, A. K., Marsh, D. R., Tilmes, S., Vitt, F., Bardeen, C. G., McInerny, J., Liu, H.-L., Solomon, S. C., Polvani, L. M., Emmons, L. K., Lamarque, J.-F., Richter, J. H., Glanville, A. S., Bacmeister, J. T., Phillips, A. S., Neale, R. B., Simpson, I. R., DuVivier, A. K., Hodzic, A., and Randel, W. J.: TheWhole Atmosphere Community ClimateModel Version 6 (WACCM6), J. Geophys. Res.-Atmos., 124, 12380–12403, https://doi.org/10.1029/2019JD030943, 2019.

Jones, A., Haywood, J. M., Scaife, A. A., Boucher, O., Henry, M., Kravitz, B., Lurton, T., Nabat, P., Niemeier, U., Séférian, R., Tilmes, S., and Visioni, D.: The impact of stratospheric aerosol intervention on the North Atlantic and Quasi-Biennial Oscillations in the Geoengineering Model Intercomparison Project (GeoMIP) G6sulfur experiment, Atmos. Chem. Phys., 22, 2999–3016, https://doi.org/10.5194/acp-22-2999-2022, 2022.

Keeble, J., Braesicke, P., Abraham, N. L., Roscoe, H. K., and Pyle, J. A.: The impact of polar stratospheric ozone loss on Southern Hemisphere stratospheric circulation and climate, Atmos. Chem. Phys., 14, 13705–13717, https://doi.org/10.5194/acp-14-13705-2014, 2014.

Kolstad, E. W., Lee, S. H., Butler, A. H., Domeisen, D. I. V., & Wulff, C. O.: Diverse surface signatures of stratospheric polar vortex anomalies. Journal of Geophysical Research: Atmospheres, 127, e2022JD037422, https://doi.org/10.1029/2022JD037422, 2020.

Kretschmer, M., Zappa, G., and Shepherd, T. G.: The role of Barents–Kara sea ice loss in projected polar vortex changes, Weather Clim. Dynam., 1, 715–730, https://doi.org/10.5194/wcd-1-715-2020, 2020.

Kult-Herdin, J., T. Sukhodolov, G. Chiodo, R. Checa-Garcia, and H. Rieder: The impact of different CO2 and ODS levels on the mean state and variability of the springtime Arctic stratosphere, Environmental Research Letters, DOI:10.1088/1748-9326/acb0e6, 2023.

Liu, X., Ma, P.-L., Wang, H., Tilmes, S., Singh, B., Easter, R. C., Ghan, S. J., and Rasch, P. J.: Description and evaluation of a new four-mode version of the Modal Aerosol Module (MAM4) within version 5.3 of the Community Atmosphere Model, Geosci. Model Dev., 9, 505–522, https://doi.org/10.5194/gmd-9-505-2016, 2016.

MacMartin, D. G., Visioni, D., Kravitz, B., Richter, J., Felgenhauer, T., Lee, W. R., Morrow, D. R., Parson, E. A., Sugiyama, M.:. Scenarios for modeling solar radiation modification. Proceedings of the National Academy of Sciences, 119(33). https://doi.org/10.1073/pnas.2202230119, 2022.

Manzini, E., Karpechko, A. Y., & Kornblueh, L.: Nonlinear response of the stratosphere and the North Atlantic-European climate to global warming. Geophysical Research Letters, 45, 4255– 4263, https://doi.org/10.1029/2018GL077826, 2018.

Maycock, A. C., Joshi, M. M., Shine, K. P., & Scaife, A. A.: The circulation response to idealized changes in stratospheric water vapor. Journal of Climate, 26(2), 545–561. https://doi.org/10.1175/JCLI-D-12-00155.1, 2013.

McCusker, K. E., Battisti, D. S., & Bitz, C. M.: Inability of stratospheric sulfate aerosol injections to preserve the West Antarctic Ice Sheet. Geophysical Research Letters, 42(12), 4989–4997, 2015.

Seabrook, M., Smith, D. M., Dunstone, N. J., Eade, R., Hermanson, L., Scaife, A. A., & Hardiman, S. C.: Opposite impacts of interannual and decadal Pacific variability in the extratropics. Geophysical Research Letters, 50, e2022GL101226, https://doi.org/10.1029/2022GL101226, 2023.

Thompson, D. W. J., M. P. Baldwin, and S. Solomon: Stratosphere–Troposphere Coupling in the Southern Hemisphere. J. Atmos. Sci., 62, 708–715, https://doi.org/10.1175/JAS-3321.1, 2005.

Thompson, D. W. J., & Wallace, J. M.: Annular modes in the extratropical circulation. Part I: Month-to-month variability. Journal of Climate, 13(5), 1000–1016. https://doi.org/10.1175/1520-0442(2000)01360;1000:amitec62;2.0.co;2, 2000.

Tilmes, S., Richter, J. H., Kravitz, B., MacMartin, D. G., Glanville, A. S., Visioni, D., Kinnison, D. E., and Müller, R.: Sensitivity of total column ozone to stratospheric sulfur injection strategies, Geophys. Res. Lett., 48, e2021GL094058, https://doi.org/10.1029/2021GL094058, 2021.

Tilmes, S., Visioni, D., Jones, A., Haywood, J., Séférian, R., Nabat, P., Boucher, O., Bednarz, E. M., and Niemeier, U.: Stratospheric ozone response to sulfate aerosol and solar dimming climate interventions based on the G6 Geoengineering Model Intercomparison Project (GeoMIP) simulations, Atmos. Chem. Phys., 22, 4557–4579, https://doi.org/10.5194/acp-22-4557-2022, 2022.

Walz, R., H. Garny, and T. Birner: Stratospheric Modulation of Tropical Upper-Tropospheric Warming-Induced Circulation Changes in an Idealized General Circulation Model. J. Atmos. Sci., 80, 611–631, https://doi.org/10.1175/JAS-D-21-0232.1, 2023.

Wang, S., E. P. Gerber, and L. M. Polvani: Abrupt circulation responses to tropical upper-tropospheric warming in a relatively simple stratosphere-resolving AGCM. J. Climate, 25, 4097–4115, https://doi.org/10.1175/JCLI-D-11-00166.1, 2012.

Visioni, D., Bednarz, E. M., Lee, W. R., Kravitz, B., Jones, A., Haywood, J. M., and MacMartin, D. G.: Climate response to off-equatorial stratospheric sulfur injections in three Earth system models – Part 1: Experimental protocols and surface changes, Atmos. Chem. Phys., 23, 663–685, https://doi.org/10.5194/acp-23-663-2023, 2023a.

Visioni, D., Bednarz, E. M., MacMartin, D. G., Kravitz, B., Goddard, P.: The choice of baseline period influences the assessments of the outcomes of Stratospheric Aerosol Injection, Earth's Future, 2023b (submitted).

Zhang, Y., MacMartin, D. G., Visioni, D., Bednarz, E., and Kravitz, B.: Introducing a Comprehensive Set of Stratospheric Aerosol Injection Strategies, EGUsphere [preprint], https://doi.org/10.5194/egusphere-2023-117, 2023.

Potential non-linearities in the high latitude circulation and ozone response to Stratospheric Aerosol Injection

Ewa M. Bednarz[1,2,3], Daniele Visioni[3,4], Amy H. Butler[2], Ben Kravitz[5,6], Douglas G. MacMartin[3], Simone Tilmes[4]

1. Cooperative Institute for Research in Environmental Sciences (CIRES), University of Colorado Boulder, Boulder, CO, USA
2. NOAA Chemical Sciences Laboratory (NOAA CSL), Boulder, CO, USA
3. Sibley School of Mechanical and Aerospace Engineering, Cornell University, Ithaca, NY, USA
4. Atmospheric Chemistry Observations and Modelling (ACOM), National Center for Atmospheric Research (NCAR), Boulder, CO, USA
5. Department of Earth and Atmospheric Sciences, Indiana University, Bloomington, IN, USA
6. Atmospheric Sciences and Global Change Division, Pacific Northwest National Laboratory, Richland, WA, USA

Key points

- Impacts of Stratospheric Aerosol Injection (SAI) depend on how much surface cooling is to be achieved.

- High latitude circulation, ozone and modes of extratropical variability can vary non-linearly with the SAI-induced global surface cooling

- These potential non-linearities may add to uncertainties in projections of regional surface impacts under SAI

Abstract

The impacts of Stratospheric Aerosol Injection (SAI) on the atmosphere and surface climate depend on when and where the sulfate aerosol precursors are injected, as well as on how much surface cooling is to be achieved. We use a set of CESM2(WACCM6) SAI simulations achieving three different levels of global mean surface cooling and demonstrate that unlike some direct surface climate impacts driven by the reflection of solar radiation by sulfate aerosols, the SAI-induced changes in the high latitude circulation and ozone are more complex and could be non-linear. This manifests in our simulations by disproportionally larger Antarctic springtime ozone loss, significantly larger intra-ensemble spread of the Arctic stratospheric jet and ozone responses, and non-linear impacts on the extratropical modes of surface climate variability under the strongest-cooling SAI scenario compared to the weakest one. These potential non-linearities may add to uncertainties in projections of regional surface impacts under SAI.

Plain Language Summary

The injection of reflective aerosols, or their precursors, into the lower stratosphere (Stratospheric Aerosol Injection, SAI) has been proposed as a temporary measure to offset some of the adverse impacts of climate change whilst atmospheric concentrations of greenhouses are being stabilised and, ultimately, reduced. The impacts of SAI on the atmosphere and surface climate would depend on when and where the sulfate aerosol precursors are injected, as well as on how much surface cooling is to be achieved. Here we analyze SAI impacts on stratospheric climate and ozone in a set of Earth system model simulations under varying magnitudes of the SAI-induced global mean cooling. We demonstrate that unlike some of the direct surface climate impacts from the reflection of solar radiation by sulfate aerosols, the SAI-induced changes in stratospheric circulation, chemistry and climate are more complex, with the model simulations pointing towards more non-linear behaviour of the high latitude circulation and ozone under higher SAI scenarios.

These potential non-linearities may add to uncertainties in projections of regional surface impacts under SAI.

1. Introduction

The injection of reflective aerosols, or their precursors, into the lower stratosphere (Stratospheric Aerosol Injection, SAI) has been proposed as a temporary measure to offset some of the adverse impacts of climate change whilst atmospheric concentrations of greenhouses are being stabilised and, ultimately, reduced. Research in support of informed decision making for potential future SAI requires a detailed assessment of the effectiveness and efficiency of SAI as well as the associated side-effects. The latter include the warming in the tropical lower stratosphere from the absorption of radiation by sulfate aerosols, which can then impact the large-scale Brewer Dobson Circulation (BDC) and stratospheric polar jets, driving changes in both transport of stratospheric ozone and the mid and high latitude surface climate via stratosphere-troposphere coupling (e.g., Ferraro et al., 2015; McCusker et al., 2015; Jones et al., 2022; Banerjee et al., 2021; Bednarz et al., 2022; Tilmes et al., 2021; 2022). In addition, the activation of atmospheric halogens on aerosol surfaces can accelerate catalytic ozone depletion and, thus, slow down the ongoing recovery of stratospheric ozone layer to its pre-1980 levels (e.g. Tilmes et al., 2021; 2022).

The effectiveness of SAI in reducing surface temperatures and mitigating regional climate change will depend on where and when the aerosol precursors are injected (Visioni et al., 2023a; Bednarz et al., 2023a; 2023b; Zhang et al, 2023). In addition, the effectiveness of parallel GHG emission reductions will determine the overall magnitude of SAI needed to maintain or cool the temperatures to a desired level, and the resulting SAI impacts will thus also depend on this desired temperature target (MacMartin et al., 2022; Visioni et al., 2023b). Visioni et al., (2023b) analysed some of the surface climate responses in a set of SAI simulations using the same injection strategy (i.e. the same location of SO_2 injections) but achieving different levels of global mean surface cooling (though different total magnitudes of SAI), and showed that many of the resulting changes scale broadly linearly with the amount of SAI-induced cooling.

Though the direct radiative changes at the surface behave quasi linearly with the amount of SAI, the behaviour of the stratosphere-troposphere coupled circulation has been shown to be non-linear or regime-like in character in response to external forcings, both idealised thermal forcings and climate change (Charney and Drazin, 1961, Wang et al., 2012; Manzini et al., 2018; Walz et al., 2023), and thus harder to predict. Similarly, in the stratosphere the concentrations of chemical tracers like ozone are driven by a range of chemical and dynamical processes, the relative contribution of which could change under SAI. Here we extend the work of Visioni et al., (2023b) by analysing the impacts of SAI on stratospheric climate and ozone under varying magnitudes of global mean cooling. We demonstrate that while the tropical stratospheric changes behave largely linearly, the resulting high latitude dynamical responses to SAI are more complex and could vary non-linearly with increasing magnitudes of SAI. These in turn could lead to non-linear impacts on high-latitude climate and ozone that may add to uncertainties in projections of some regional surface impacts under SAI.

2. Methods

We use the CESM2(WACCM6) earth system model (Gettelman et al., 2019; Danabasoglu et al., 2020) with interactive modal aerosol microphysics (MAM4, Liu et al., 2016) and interactive middle atmosphere chemistry (Davis et al., 2023). The horizontal resolution is 1.25° longitude by 0.9° latitude, with 70 vertical levels in hybrid-pressure coordinates up to ~140 km. The simulations used are introduced in MacMartin et al. (2022) and described in detail in Visioni et al. (2023b). The Coupled Model Intercomparison Project Phase 6 (CMIP6) Shared Socioeconomic Pathway SSP2-4.5 experiment is chosen as a background emission scenario. In all SAI simulations SO_2 is injected at 21.5 km at four off-equatorial latitudes – 30°S, 15°S, 15°N, 30°N – using a feedback algorithm that controls for the global mean surface temperature as well as its large scale interhemispheric and equator-to-pole gradients.

Three SAI scenarios, each consisting of three ensemble members, start in 2035 and continue until 2069 inclusive. 'SAI1.5' maintains the above three temperature objectives at the levels corresponding to 1.5°C above preindustrial conditions, with total SO_2 injection of 8.6 Tg-SO_2/yr averaged over the last 20 years of simulations. This baseline was chosen as corresponding to the 2020-2039 mean of the CESM2 SSP2-4.5 simulation ('BASE1.5'). 'SAI1.0' and 'SAI0.5' are similar to SAI1.5 but aim to achieve more surface cooling by injecting more SO_2 (17.0 and 25.6 Tg-SO_2/yr averaged over the last 20 years of simulations, respectively), with the desired global mean surface temperatures of 1.0°C and 0.5°C above preindustrial conditions, respectively; these baseline periods correspond in CESM2 to the mean over the 2008-2027 and 1993-2012 periods, respectively.

We analyse the last 20-years of the simulations (2050-2069) and compare them against the same period of the control SSP2-4.5 simulation and/or against the same BASE1.5 baseline period representative of quasi-present day conditions. This avoids complications from the different contributions of the concurrent changes in GHGs and ozone depleting substances if the SAI responses are compared against each individual baseline period instead (see Visioni et al. 2023b for more discussion on the role of the choice of baseline period).

3. Changes in tropical stratospheric climate

The introduction of sulfate aerosols into the stratosphere and the resulting scattering of a portion of coming solar radiation reduces tropical tropospheric temperatures, with the strongest reduction, by design, found in SAI0.5 and smallest in SAI1.5 (Fig. 1a). In the lower stratosphere, the absorption of the portion of the outgoing terrestrial and incoming solar radiation by sulfate increases local temperatures. The magnitude of this effect is in tight linear relationship with the global mean surface cooling in each of the SAI simulation, with R^2 = 0.95 for the goodness of fit of the individual ensemble members and R^2=1.00 for the fit to the ensemble means (Fig. 1e).

The SAI-induced lower stratospheric warming drives changes in the large-scale circulation, decelerating the shallow branch of the BDC and accelerating the deep branch (see Fig. 1b for changes in residual vertical velocities; by mass continuity, these are closely related to changes in horizontal velocities). Changes in the large-scale transport modulate stratospheric distribution of chemical tracers, most importantly ozone. In the tropics (Fig. 1d), this increases ozone in the tropical lower stratosphere (from reduced input of ozone-poor tropospheric air) and decreases ozone above it at ~30 hPa (from enhanced input of lower stratospheric air with lower ozone concentrations). Climatologically, the absorption of solar radiation by ozone constitutes the dominant source of heat in the stratosphere and, thus, any changes in its concentration act to further modulate stratospheric temperatures. A tight correlation between SAI-induced changes in tropical temperatures, ozone and transport was shown to hold also in a multi-model context (Bednarz et al., 2023a). In the extratropics, SAI-induced strengthening of the BDC enhances ozone transport from its tropical photochemical production region to higher latitudes, thereby increasing total column levels in the mid and high latitudes (See Section 5). Finally, the SAI-induced warming around the cold point tropical tropopause allows more water vapour to enter the stratosphere (Fig. 1c), and this acts to offset some of the direct surface cooling as water vapour traps a portion of the outgoing terrestrial radiation (Bednarz et al., 2023b). Increased stratospheric water vapour also modulates the rates of chemical ozone loss, as well as provides additional stratospheric cooling.

Overall, the magnitudes of these responses scale linearly with increasing magnitude of SAI. Whilst a strong linear relationship was found for the magnitudes of lower stratospheric warming (Fig. 1e) and BDC changes (Fig. 1f), some deviations from a linear relationship begin to emerge for changes in lower stratospheric water vapour (Fig. 1g) and ozone (Fig. 1h) under the strongest SAI scenario. The latter may reflect certain nonlinearities in aerosol microphysics under high inject rates (Visioni et al., 2023b) or a contribution of the apparent non-linearities at higher latitudes (Sections 4 and 5).

4. High latitude dynamical response

4.1. Stratosphere

The enhancement of the meridional temperature gradients as the result of SAI-induced warming in the tropical lower stratosphere drives strengthening of the stratospheric jets in both hemispheres, and the magnitude of the response increases with the magnitude of SO_2 injection (Fig. 2a-c). The degree of linearly of this response with respect to the amount of global mean surface cooling depends on the season under analysis.

In the Southern Hemisphere (SH) during austral winter (Fig. 2e), where the very strong climatological jet prohibits much planetary wave propagation and, thus, any changes are mainly radiatively driven via the thermal wind relationship, a strong linear relationship (R^2=0.94 for the fit to the ensemble means of SAI1.5, SAI1.0 and SAI0.5) is found between the magnitude of the SH jet strengthening and the global mean surface cooling. However, in spring (SON, Fig. 2g), when interactions with both planetary waves and with the SAI-induced ozone depletion within the polar vortex (Section 5) can occur, a more non-linear relationship emerges: the jet strengthening in the largest SAI scenario (SAI0.5) is disproportionally larger than that inferred for SAI1.0 and SAI1.5 (9 m/s, 4 m/s and 2 m/s, respectively). For the Northern Hemisphere (NH) during winter (DJF, Fig. 2d) the apparent non-linearity is even stronger: the NH jet strengthening simulated in SAI0.5 is also disproportionally larger than that in SAI1.0 and SAI1.5 (8 m/s, 4 m/s and 3 m/s, respectively), and is also characterised by a much larger spread in the zonal wind responses simulated across the individual ensemble members (blue crosses) than it is the case for either SAI1.0 and SAI1.5.

Non-linearity of the NH polar vortex response has been previously found in response to increased CO_2 forcing (Manzini et al. 2018) and to idealized heating in a dry dynamical model (Wang et al. 2012, Walz et al. 2023), and may be related to either differences in tropospheric wave forcing that arise from non-linear changes in sea ice (Kretschmer et al., 2020) or sea surface temperatures, or to regime-like behaviour in the stratospheric planetary wave guide (Walz et al. 2022).

4.2. Northern Hemisphere troposphere

Through wave-mean flow interactions, extratropical stratospheric wind changes can propagate down to the troposphere and affect surface climate (e.g. Baldwin and Dunkerton, 2001; Thompson and Wallace 2000); in the NH this coupling maximises in winter. In the absence of SAI for the SSP2-4.5 scenario, increasing tropospheric temperatures in CESM2(WACCM6) cause strengthening of zonal winds in the subtropics and weakening of zonal winds in the Arctic region (Figure S3). Thus, a comparison of SAI against SSP2-4.5 for the same future time period reflects in part the response to climate change itself (Fig. S4). In order to better isolate the influence of SAI-induced changes in the stratosphere, Figure 3 shows the tropospheric SAI responses compared to the BASE1.5 period (i.e. present day) instead.

We find that the NH stratospheric westerly changes compared the present-day period only propagate down to the troposphere under the strongest SAI scenario (SAI0.5), Fig. 3a-c. The surface response in NH winter manifests as the pattern of sea-level pressure changes projecting on the positive phase of the North Atlantic

Oscillation (NAO) (Fig. 3d-f) diagnosed also from each individual ensemble member of SAI0.5 (Fig. S5 and S6). The positive NAO response drives a dynamically induced warming over northern Eurasia, which is large enough to locally offset the large-scale cooling from the reduction in the global mean surface temperatures (Fig. S6). In contrast, no significant tropospheric jet strengthening or NAO-like sea-level pressure response is found in the two smaller SAI scenarios (SAI1.0 and SAI1.5. Fig 3a-f). While the pattern of sea-level pressure changes in SAI1.0 resembles that of a positive NAO, the ensemble mean response is very weak and not statistically significant, with little agreement between the responses simulated across the individual ensemble members (Fig. S5 and S6).

The strength of the stratosphere-troposphere coupling can be assessed by correlating the changes in the NH stratospheric jet with the NAO index for each of the ensemble members and scenarios. Following our earlier work (Bednarz et al., 2023a) we calculate the model NAO index as the difference in sea-level pressure between the Atlantic mid-latitudes (280°E-360°E, 30°N-60°N) and the Arctic polar cap (70°N-90°N, all longitudes). Over the 20-year mean period analysed here, we find a strong relationship between the strength of the stratospheric winds and surface NAO responses for the three ensemble members of the strongest SAI scenario (SAI0.5), with stronger stratospheric westerly anomalies being associated with more positive NAO values (blue points in Fig. 3g). In contrast, no such relationship can be inferred for the responses in the individual ensemble members of the two smaller SAI scenarios (SAI1.0 and SAI1.5). An analysis of temporal evolution of the responses reveals that the apparent non-linearity emerges toward the end of the simulations (Fig. S8), where the injection rates are highest.

Such apparent nonlinearity in the NH surface responses may result from the non-linearity in the stratospheric jet response itself (Section 4.1), or from non-linearities in the tropospheric circulation or sea ice and sea surface temperatures that either discourage or promote the canonical downward coupling from the stratosphere on the NAO (Kolstad et al., 2022). Another possibility is that the enhanced stratosphere-troposphere coupling under the largest SAI scenario arises because the response is only for that case strong enough to emerge from the background natural variability, which is particularly high in the NH winter (e.g. Bittner et al., 2016; DallaSanta and Polvani, 2022).

4.3. Southern Hemisphere troposphere

Anomalies in the SH stratospheric jet can also propagate down to the troposphere and affect the SH surface climate; such stratospheric influence tends to maximise in austral spring and summer (SON and DJF). We find that the SAI-induced westerly stratospheric anomalies do not propagate down to the surface in any of the SAI simulations (Fig. 3h-j). This is the case even for the strongest SAI0.5 scenario (Fig. 3j) that shows disproportionally larger stratospheric jet perturbation in spring than the smaller SAI1.0 and SAI1.5. We would expect a strengthened SH stratospheric jet in austral spring to lead to a later than average seasonal transition of the polar vortex and an associated shift towards the positive phase of the Southern Annular Mode (SAM) in austral summer (e.g. Thompson et al., 2005). Instead, all SAI scenarios give rise to a pattern of sea-level pressure changes projecting onto the negative phase of SAM, inferred both from DJF (Fig. 3h-j) and yearly mean (Fig. S9) data, with no clear linear relationship between the strength of the SAM-like sea-level pressure pattern and the SAI magnitude. This suggests that factors other than the magnitude of the injection, especially the meridional distribution of sulfate in the stratosphere (e.g. Bednarz et al., 2022, GRL), are more important in determining the SH high latitude tropospheric and surface response to SAI.

5. Impacts on Arctic and Antarctic ozone

5.1 Antarctic ozone

In austral spring, the SH high latitude ozone columns decrease under all three SAI scenarios compared to the same period of SSP2-4.5 because of the enhancement of heterogeneous halogen activation on sulfate and the resulting catalytic stratospheric ozone depletion inside the Antarctic polar vortex (Fig. 4a). In addition, the strengthening of the polar vortex inhibits mixing with the more ozone-rich mid-latitude air, thereby further reducing polar ozone levels. We find similar Antarctic (65°S-90°S) ozone losses of 26 DU (= 9%) and 30 DU (= 11%) for the two lower SAI scenarios, SAI1.5 and SAI1.0, respectively. In contrast, a significantly higher Antarctic ozone loss of 43 DU (= 15%) is found for the largest SAI0.5 scenario.

A tight linear relationship is found between the polar ozone column reduction and the strengthening of the Antarctic polar vortex across the simulations (Fig. 4d), and also between the ozone changes and the increased aerosol surface area densities (SAD, Fig. 4g). A stronger and colder polar vortex under more aggressive SAI scenario accelerates halogen activation on sulfate as well as delays final vortex break up and the resulting termination of the catalytic ozone loss by in-mixing of the mid-latitude NO_2-rich, air; both factors enhance Antarctic ozone loss under SAI. Conversely, enhanced ozone depletion under higher sulfate surface area densities results in dynamical impact on the polar vortex itself, cooling the polar stratosphere and strengthening the stratospheric zonal winds (e.g. Keeble et al., 2014). The strong linear relationship between these quantities under varying SAI levels demonstrates how the same processes operate under all three SAI scenarios. The cause of the apparent non-linearity and thus the significantly higher magnitude of the Antarctic springtime ozone loss in SAI0.5 compared to SAI1.0 and SAI1.5 is thus dynamical in origin, in line with the significantly larger strengthening of the polar vortex in SAI0.5 than the other two scenarios.

5.2 Arctic ozone

Unlike in the SH, the NH ozone column largely increases under SAI during boreal winter and spring (Fig. 4b-c) due to the SAI-induced changes in the BDC and the resulting ozone transport (Section 3). Owing to the Arctic vortex being climatologically weaker and more variable than its SH counterpart, the chemical impacts from the SAI-induced enhancement of the heterogenous halogen processing on the elevated SAD are generally smaller. They do however still contribute to the simulated column ozone changes, alongside dynamical impacts from the reductions in mixing under the strengthened Arctic polar vortex.

Consistently, SAI1.5 shows increased NH winter total ozone columns in the mid- and high latitudes up to ~75°N, with a small total column ozone decrease poleward. For SAI1.0, the total column ozone changes are positive everywhere and larger in magnitude than for SAI1.5; this indicates that the impact of SAI on the strength of the BDC dominates over chemically driven ozone reductions in this scenario. In spring, ozone columns increase throughout the NH in the ensemble mean for both SAI1.5 and SAI0.5, albeit with larger variability between the individual ensemble members than during winter (dashed lines in Fig. 4b-c).

An interesting picture emerges for the largest SAI0.5 scenario: whilst ozone columns increase in winter in the ensemble mean throughout the NH, the magnitude of the response is sharply reduced in the Arctic region, with substantially larger variability between the individual ensemble members. In fact, one ensemble member of SAI0.5 shows the strongest decrease in Arctic ozone at the pole from all the SAI simulations and members. The large intra-ensemble variability continues into spring, with individual members of SAI0.5 showing both the most positive and the most negative Arctic column ozone perturbations. The large springtime ozone variability extends to the mid-latitudes, as anomalies in polar ozone mix-in with the mid-latitude air following the vortex break-up. The contrastingly different ozone behaviour in SAI0.5 is concurrent with the strongest and more non-linear high latitude dynamical response identified above (Section 4.1-2). Owing to the interplay of various dynamical and chemical processes in the

Arctic, with its opposing impacts on total ozone column, the previously identified linear relationship between changes in the Antarctic ozone, polar vortex and sulfate SAD (Fig. 4d,g) is generally not found in the Arctic during winter(Fig. 5e,h). The inverse relationship between changes in polar ozone and vortex strength is only apparent under the strongest SAI0.5 scenario, facilitated by the much larger variability between the ensemble members.

Recent studies highlighted the role of dynamical and chemical ozone reductions inside the Arctic polar vortex in modulating the northern polar jet dynamics (Friedel et al., 2022a; 2022b; Kult-Herdin et al., 2023). However, it was also demonstrated that this ozone feedback, as manifested by the inverse relationship between polar ozone and jet strength, is only found under the present-day (i.e. high) levels of ozone-depleting substances where ozone variability is larger (Kult-Herdin et al., 2023). It is possible that the same occurs under SAI, i.e. the feedback from interactive ozone in our runs only starts to play a significant role in contributing to the polar vortex behaviour under the strongest SAI0.5 scenario, where the aerosol SAD and, thus, chemical ozone depletion is largest.

In spring, the inverse relationship between polar ozone and the vortex strength (Fig. 4f) or SAD (Fig. 4i) emerges for each individual SAI scenario. This indicates that the differences in springtime ozone responses across the different SAI scenario (Fig. 4c) are driven predominantly by the SAI-induced changes in the BDC, whereas the intra-ensemble spread in each scenario is associated more linearly with chemical-dynamical feedbacks.

6. Summary and discussion

The impacts of Stratospheric Aerosol Injection on the atmosphere and surface climate would depend on when and where the sulfate aerosol precursors are injected, as well as on how much surface cooling is to be achieved. Here we extend our recent work that explored the linearity of some of the direct surface climate impacts in a set of CESM2(WACCM6) SAI simulations achieving three different levels of a global mean surface cooling (Visioni et al., 2023b). We demonstrate that unlike some of the direct surface climate impacts from the reflection of solar radiation by sulfate aerosols, the SAI-induced changes in stratospheric circulation, chemistry and climate are more complex, with the model simulations pointing towards more non-linear behaviour of the high latitude circulation and ozone under higher SAI scenarios.

We find that the SAI-induced changes in the tropical stratospheric temperatures, upwelling, water vapour and ozone scale roughly linearly with the magnitude of global mean cooling in CESM2 under the multi-objective SAI strategy used. A significantly more non-linear behaviour is found for the associated extratropical stratospheric zonal wind responses, in particular in seasons when the wave-mean flow coupling plays an important role. In those cases, a disproportionally stronger westerly jet anomaly is simulated for the largest SAI scenario (SAI0.5) compared to the more modest ones. In the SH, this is associated with markedly stronger (~50%) Antarctic springtime ozone depletion in SAI0.5. In the NH, the non-linearity manifests in part as the significantly larger intra-ensemble spread of the SAI-induced changes in the stratospheric jet strength and Arctic ozone columns in SAI0.5. The scenario also gave rise to much stronger NH stratosphere-troposphere coupling, facilitating the propagation of the stratospheric westerly down to the surface in the form of the positive North Atlantic Oscillation, which was otherwise not reproduced for the two smaller SAI scenarios. Regarding impacts on the Southern Annular Mode, the analogous propagation of the SH polar vortex strengthening to the troposphere is not found under any SAI scenario; this points to other factors like the meridional distribution of sulfate in the stratosphere (and thus the location of the injection) being more important in determining the SAI impacts in the region.

The results highlight the complexity of the impacts of SAI on the stratospheric climate, high latitude circulation and stratospheric ozone, including the complex interplay of various chemical, radiative and dynamical processes. Dynamical mechanisms for abrupt regime changes driving the dynamical responses to thermal perturbations were previously found in idealised models (e.g. Wang et al., 2012; Walz et al., 2023). Whether these mechanisms apply also to more complex climate models is still not well understood, but non-linearities in the stratospheric jet response to different levels of global warming have previously been found (Manzini et al., 2018). The role of chemically driven Arctic and Antarctic ozone reductions in modulating the polar vortex behaviour has also been highlighted as a potentially important feedback mechanism that is still not sufficiently understood (Keeble et al., 2014; Friedel et al., 2022a; 2022b; Kult-Herdin et al., 2023). Here evidence of such feedback was shown to be particularly strong under the largest SAI scenario, i.e. when the higher stratospheric aerosol levels drive larger chemical ozone losses that can then module the polar vortex. Finally, though not examined in detail in this study, changes in stratospheric water vapour have also been shown to drive changes in the high latitude circulation (Maycock et al., 2013; Seabrook et al., 2023), as well as enhance catalytic ozone loss (e.g. Tilmes et al., 2021), but uncertainties remain as to the details of such responses. Since SAI-induced lower stratospheric warming also drives significant increases in stratospheric water vapour, this process constitutes an additional source of uncertainty to the overall SAI impacts in the high latitudes.

We note that our results could be model dependent. In addition, with three ensemble members per experiment, a rigorous assessment of the origin of these dynamical differences is beyond the scope of the current study. However, the apparent non-linear behaviour of the high latitude circulation and ozone response to SAI merits further assessment in a multi-model framework and with larger ensembles, as part of ongoing efforts in narrowing the uncertainties in the climate response to SAI.

Acknowledgements

We would like to acknowledge high-performance computing support from Cheyenne (https://doi.org/10.5065/D6RX99HX) provided by NCAR's Computational and Information Systems Laboratory, sponsored by the National Science Foundation. Support was provided by the NOAA cooperative agreement NA22OAR4320151, NOAA Earth's Radiative Budget initiative, Atkinson Center for a Sustainability at Cornell University, and by the National Science Foundation through agreement CBET-2038246. Support for BK was provided in part by the National Science Foundation through agreement SES-1754740 and the Indiana University Environmental Resilience Institute. The Pacific Northwest National Laboratory is operated for the US Department of Energy by Battelle Memorial Institute under contract DE-AC05-76RL01830.

Data access

Data used in this manuscript is available from doi: 10.5281/zenodo.7976364.

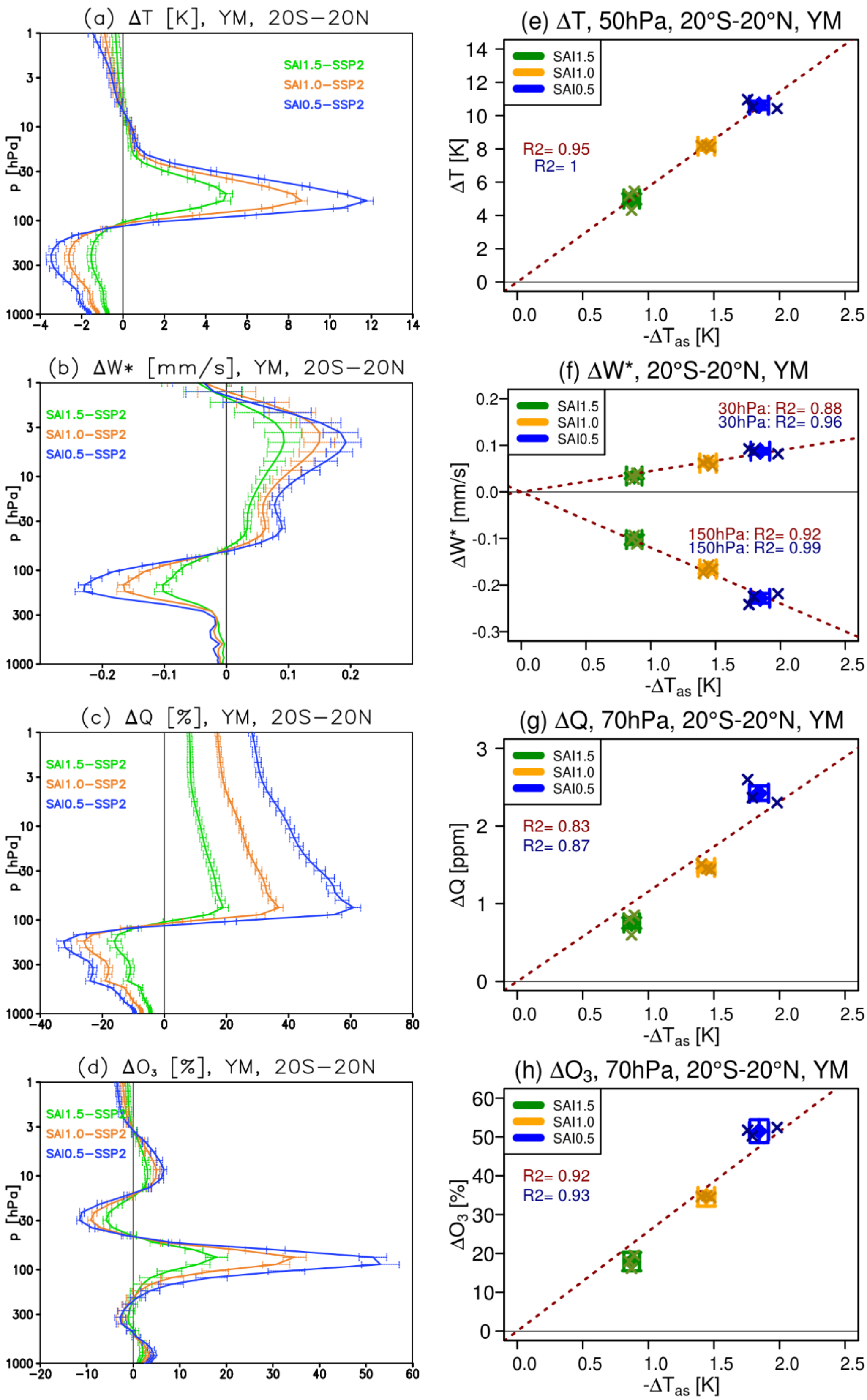

Figure 1. Left: Yearly mean changes in the ensemble mean tropical (a,e) temperatures, (b,f) TEM vertical velocity, (c,g) water vapour and (d,h) ozone for each of the SAI scenarios compared to the control SSP2-4.5 simulation for the same period (2050-2069). Error bars denote ±2 standard errors of the difference in means. Right: Scatterplot of the SAI stratospheric responses against the magnitude of the global mean surface cooling. Diamonds and whiskers indicate ensemble mean response ±2 standard error, and the crosses indicate

the responses in the individual ensemble members (compared to the ensemble mean of SSP2-4.5). Value of R^2 shown in red and blue corresponds to the value calculated for the single ensemble members and the ensemble means, respectively. See **Fig. S1** in Supplement for the analogous responses compared to the present day BASE1.5 baseline period.

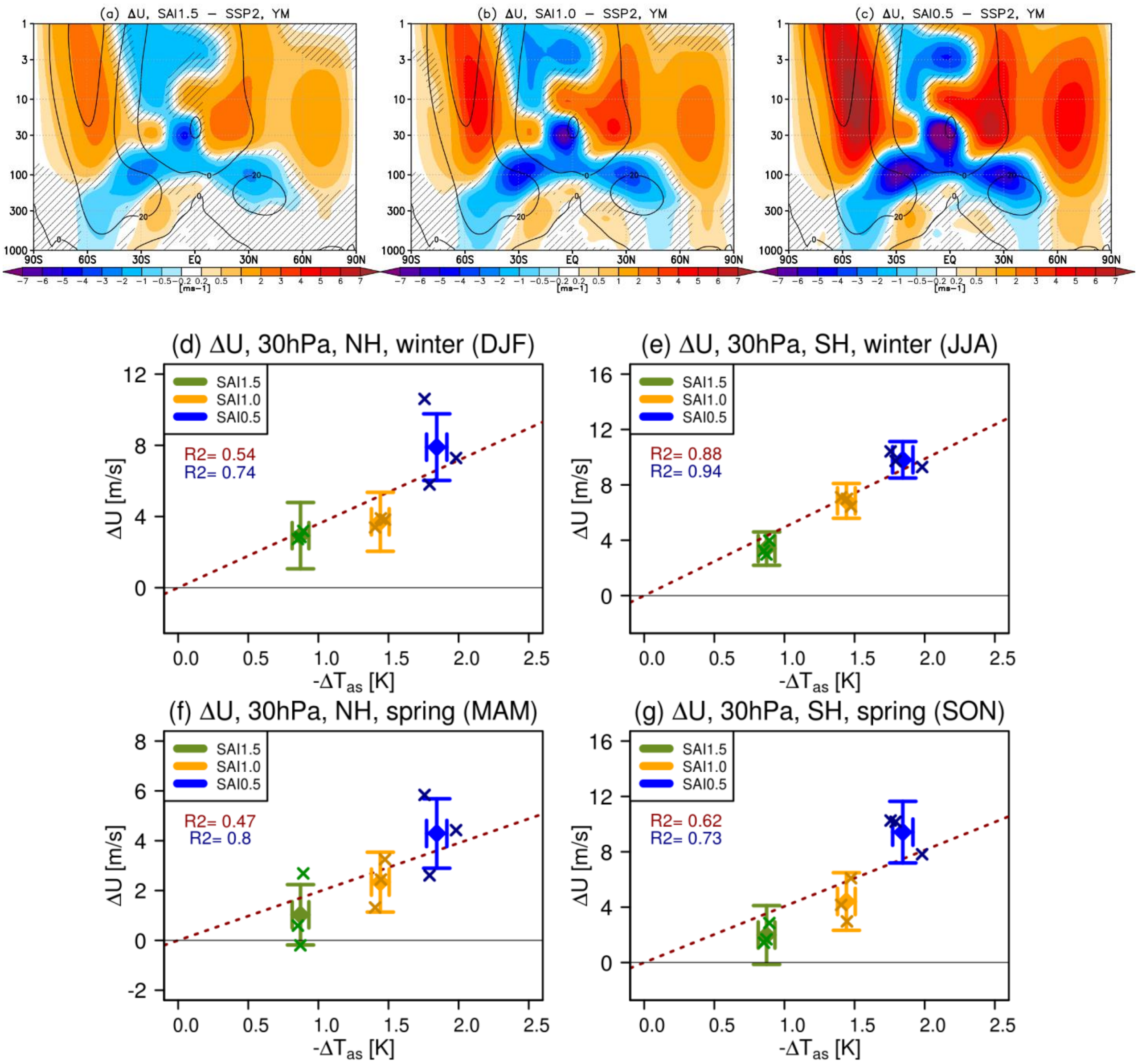

Figure 2. (a-c) Shading: yearly mean changes in zonal winds in each of the SAI simulation compared to SSP2-4.5. Contours show the values in SSP2-4.5 for reference. Hatching marks the regions where the response is not statistically significant (taken as ±2 standard error of the difference in means). (d-g) Changes in the strength of the NH (60°N, d,f) and SH (50°S, e,g) polar vortex at 30 hPa in winter (d,e) and spring (f,g) in each of the SAI scenario vs the magnitude of the global mean surface cooling compared to SSP2-4.5. Diamonds and whiskers indicate ensemble mean response ±2 standard error, and the crosses indicate the responses in the individual ensemble members (compared to the ensemble mean of SSP2-4.5). Value of R2 shown in red and blue corresponds to the value calculated for the single ensemble members and ensemble means, respectively. See **Fig. S2** in Supplement for the analogous responses compared to the present day BASE1.5 baseline period.

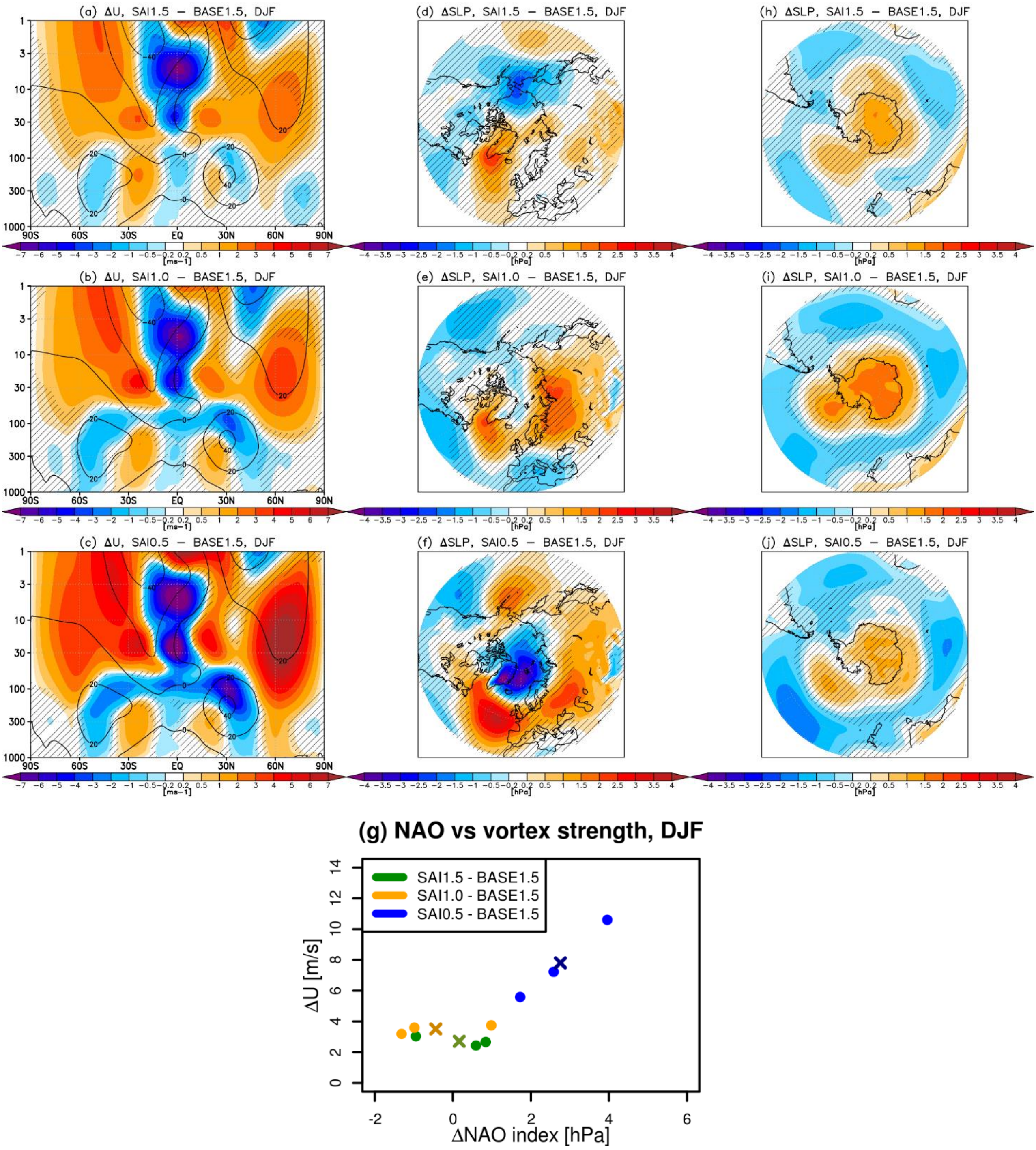

Figure 3. DJF changes in: (a-c) zonal winds, (d-f) sea-level pressures northward of 30°N, and (h-j) sea-level pressures southward of 30°S for each of the SAI scenarios compared to BASE1.5. Hatching as in Fig. 2. (g): Correlation between the DJF changes in the strength of the NH stratospheric polar vortex (60°N, 30 hPa) and the NAO sea-level pressure index for each of the SAI scenarios compared to BASE1.5. Points illustrate the responses for each of the ensemble members, and crosses the corresponding ensemble mean responses. See **Fig. S4** in Supplement for the analogous responses compared to SSP2-4.5.

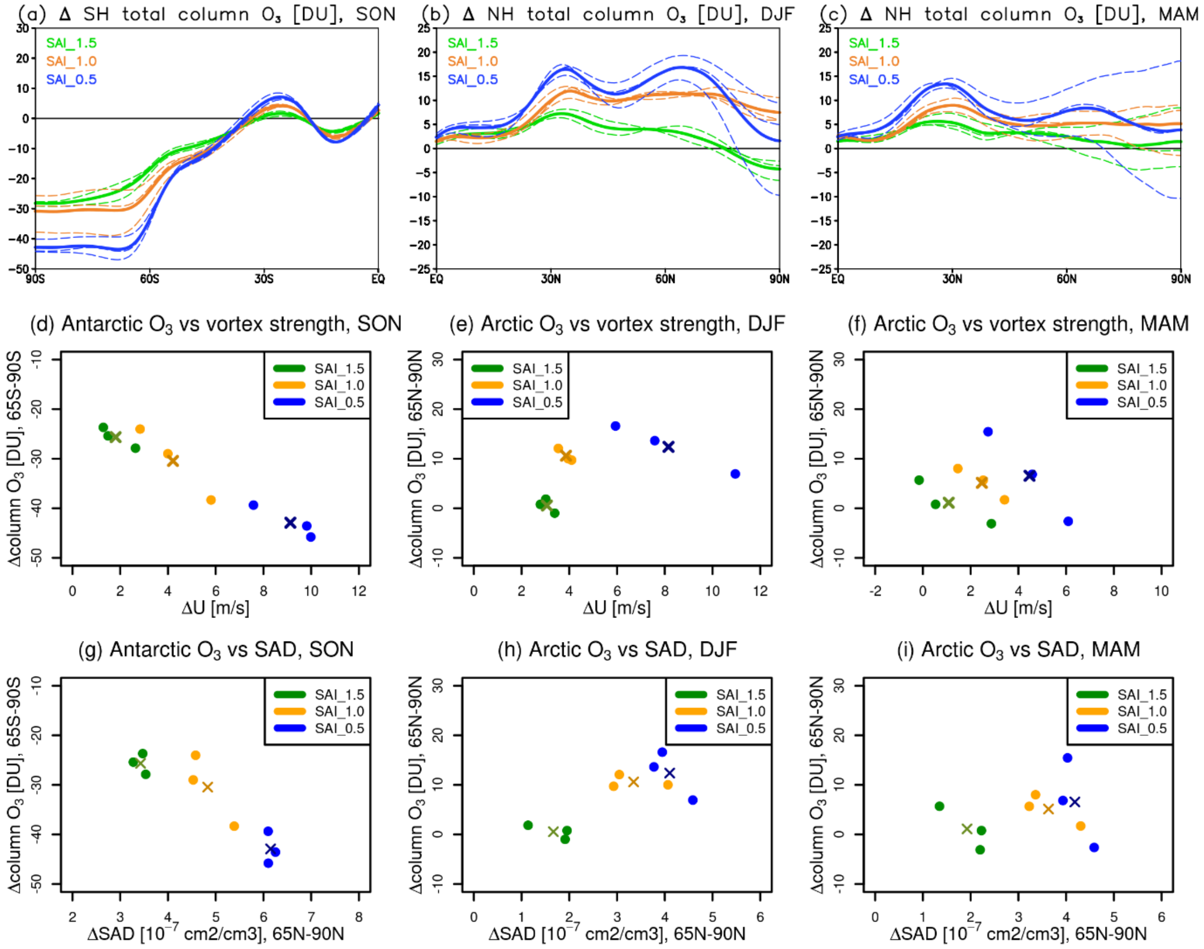

Figure 4. Impacts on the Arctic and Antarctic ozone. (a-c) Seasonal mean changes in total column ozone (left) in SON in the SH, (middle) DJF in the NH and (right) MAM in the NH for each of the SAI scenarios compared to SSP2-4.5. Thick lines denote the ensemble mean response and dashed lines the responses in each individual ensemble member (compared to the ensemble mean response in SSP2-4.5). (d-i) The correlation between seasonal mean changes in (d-f) polar ozone and stratospheric vortex strength, and between changes in (g-i) polar ozone and polar aerosol surface area density at 170 hPa. Each point represents the response in each individual ensemble member, and the cross represents the ensemble mean response.

References

Baldwin. M. P., and Dunkerton. T. J.: Stratospheric Harbingers of Anomalous Weather Regimes, Science, 294, 581-584, DOI:10.1126/science.1063315, 2001.

Banerjee, A., Butler, A. H., Polvani, L. M., Robock, A., Simpson, I. R., and Sun, L.: Robust winter warming over Eurasia under stratospheric sulfate geoengineering – the role of stratospheric dynamics, Atmos. Chem. Phys., 21, 6985–6997, https://doi.org/10.5194/acp-21-6985-2021, 2021.

Bednarz, E. M., Visioni, D., Kravitz, B., Jones, A., Haywood, J. M., Richter, J., MacMartin, D. G., and Braesicke, P.: Climate response to off-equatorial stratospheric sulfur injections in three Earth system models – Part 2: Stratospheric and free-tropospheric response, Atmos. Chem. Phys., 23, 687–709, https://doi.org/10.5194/acp-23-687-2023, 2023a.

Bednarz, E. M., Butler, A. H., Visioni, D., Zhang, Y., Kravitz, B., and MacMartin, D. G.: Injection strategy – a driver of atmospheric circulation and ozone response to stratospheric aerosol geoengineering, EGUsphere [preprint], https://doi.org/10.5194/egusphere-2023-495, 2023b.

Bednarz, E. M., Visioni , D., Richter, J. H., Butler, A. H., MacMartin , D. G.: Impact of the latitude of stratospheric aerosol injection on the Southern Annular Mode, Geophysical Research Letters, 49, e2022GL100353. https://doi.org/10.1029/2022GL100353, 2022.

Bittner, M., Schmidt, H., Timmreck, C., and Sienz, F.:Using a large ensemble of simulations to assess the Northern Hemisphere stratospheric dynamical response to tropical volcanic eruptions and its uncertainty, Geophys. Res. Lett., 43, 9324– 9332, doi:10.1002/2016GL070587, 2016.

Charney, J. G., and Drazin, P. G.: Propagation of planetary-scale disturbances from lower into upper atmosphere, Journal of Geophysical Research, 66, 83-&, 10.1029/JZ066i001p00083, 1961.

DallaSanta, K. and Polvani, L. M.: Volcanic stratospheric injections up to 160 Tg(S) yield a Eurasian winter warming indistinguishable from internal variability, Atmos. Chem. Phys., 22, 8843–8862, https://doi.org/10.5194/acp-22-8843-2022, 2022.

Danabasoglu, G., Lamarque, J.-F., Bacmeister, J., Bailey, D. A., DuVivier, A. K., Edwards, J., Emmons, L. K., Fasullo, J., Garcia, R., Gettelman, A., Hannay, C., Holland, M. M., Large, W. G., Lauritzen, P. H., Lawrence, D. M., Lenaerts, J. T. M., Lindsay, K., Lipscomb, W. H., Mills, M. J., Neale, R., Oleson, K. W., Otto-Bliesner, B., Phillips, A. S., Sacks, W., Tilmes, S., van Kampenhout, L., Vertenstein, M., Bertini, A., Dennis, J., Deser, C., Fischer, C., Fox-Kemper, B., Kay, J. E., Kinnison, D., Kushner, P. J., Larson, V. E., Long, M. C., Mickelson, S., Moore, J. K., Nienhouse, E., Polvani, L., Rasch, P. J., and Strand, W. G.: The Community Earth System Model Version 2 (CESM2), J. Adv. Model. Earth Sy., 12, e2019MS001916, https://doi.org/10.1029/2019MS001916, 2020.

Davis, N. A., Visioni, D., Garcia, R. R., Kinnison, D. E., Marsh, D. R., Mills, M. J., Richter, J. H., Tilmes, S., Bardeen, C., Gettelman, A., Glanville, A. A., MacMartin, D. G., Smith, A. K., and Vitt, F.: Climate, variability, and climate sensitivity of “Middle Atmosphere” chemistry configurations of the Community Earth System Model Version 2, Whole Atmosphere Community Climate Model Version 6 (CESM2(WACCM6)), https://doi.org/10.22541/essoar.167117634.40175082/v1, 2022.

Ferraro, A. J., Charlton-Perez, A. J., and Highwood, E. J.: Stratospheric dynamics and midlatitude jets under geoengineering with space mirrors and sulfate and titania aerosols, J. Geophys. Res.-Atmos., 120, 414–429, 2015.

Friedel, M., G. Chiodo, A. Stenke, D. Domeisen, and T. Peter: Effects of Arctic ozone on the stratospheric spring onset and its surface impact, Atmospheric Chemistry and Physics, DOI:10.5194/acp-22-13997-2022, 2022.

Friedel, M., Chiodo, G., Stenke, A. D. Domeisen, S. Fueglistaler, J. Anet, and T. Peter. Springtime arctic ozone depletion forces northern hemisphere climate anomalies. Nat. Geosci. 15, 541–547, https://doi.org/10.1038/s41561-022-00974-7, 2022.

Gettelman, A., Mills, M. J., Kinnison, D. E., Garcia, R. R., Smith, A. K., Marsh, D. R., Tilmes, S., Vitt, F., Bardeen, C. G., McInerny, J., Liu, H.-L., Solomon, S. C., Polvani, L. M., Emmons, L. K., Lamarque, J.-F., Richter, J. H., Glanville, A. S., Bacmeister, J. T., Phillips, A. S., Neale, R. B., Simpson, I. R., DuVivier, A. K., Hodzic, A., and Randel, W. J.: TheWhole Atmosphere Community ClimateModel Version 6 (WACCM6), J. Geophys. Res.-Atmos., 124, 12380–12403, https://doi.org/10.1029/2019JD030943, 2019.

Jones, A., Haywood, J. M., Scaife, A. A., Boucher, O., Henry, M., Kravitz, B., Lurton, T., Nabat, P., Niemeier, U., Séférian, R., Tilmes, S., and Visioni, D.: The impact of stratospheric aerosol intervention on the North Atlantic and Quasi-Biennial Oscillations in the Geoengineering Model Intercomparison Project (GeoMIP) G6sulfur experiment, Atmos. Chem. Phys., 22, 2999–3016, https://doi.org/10.5194/acp-22-2999-2022, 2022.

Keeble, J., Braesicke, P., Abraham, N. L., Roscoe, H. K., and Pyle, J. A.: The impact of polar stratospheric ozone loss on Southern Hemisphere stratospheric circulation and climate, Atmos. Chem. Phys., 14, 13705–13717, https://doi.org/10.5194/acp-14-13705-2014, 2014.

Kolstad, E. W., Lee, S. H., Butler, A. H., Domeisen, D. I. V., & Wulff, C. O.: Diverse surface signatures of stratospheric polar vortex anomalies. Journal of Geophysical Research: Atmospheres, 127, e2022JD037422, https://doi.org/10.1029/2022JD037422, 2020.

Kretschmer, M., Zappa, G., and Shepherd, T. G.: The role of Barents–Kara sea ice loss in projected polar vortex changes, Weather Clim. Dynam., 1, 715–730, https://doi.org/10.5194/wcd-1-715-2020, 2020.

Kult-Herdin, J., T. Sukhodolov, G. Chiodo, R. Checa-Garcia, and H. Rieder: The impact of different CO2 and ODS levels on the mean state and variability of the springtime Arctic stratosphere, Environmental Research Letters, DOI:10.1088/1748-9326/acb0e6, 2023.

Liu, X., Ma, P.-L., Wang, H., Tilmes, S., Singh, B., Easter, R. C., Ghan, S. J., and Rasch, P. J.: Description and evaluation of a new four-mode version of the Modal Aerosol Module (MAM4) within version 5.3 of the Community Atmosphere Model, Geosci. Model Dev., 9, 505–522, https://doi.org/10.5194/gmd-9-505-2016, 2016.

MacMartin, D. G., Visioni, D., Kravitz, B., Richter, J., Felgenhauer, T., Lee, W. R., Morrow, D. R., Parson, E. A., Sugiyama, M.:. Scenarios for modeling solar radiation modification. Proceedings of the National Academy of Sciences, 119(33). https://doi.org/10.1073/pnas.2202230119, 2022.

Manzini, E., Karpechko, A. Y., & Kornblueh, L.: Nonlinear response of the stratosphere and the North Atlantic-European climate to global warming. Geophysical Research Letters, 45, 4255– 4263, https://doi.org/10.1029/2018GL077826, 2018.

Maycock, A. C., Joshi, M. M., Shine, K. P., & Scaife, A. A.: The circulation response to idealized changes in stratospheric water vapor. Journal of Climate, 26(2), 545–561. https://doi.org/10.1175/JCLI-D-12-00155.1, 2013.

McCusker, K. E., Battisti, D. S., & Bitz, C. M.: Inability of stratospheric sulfate aerosol injections to preserve the West Antarctic Ice Sheet. Geophysical Research Letters, 42(12), 4989–4997, 2015.

Seabrook, M., Smith, D. M., Dunstone, N. J., Eade, R., Hermanson, L., Scaife, A. A., & Hardiman, S. C.: Opposite impacts of interannual and decadal Pacific variability in the extratropics. Geophysical Research Letters, 50, e2022GL101226, https://doi.org/10.1029/2022GL101226, 2023.

Thompson, D. W. J., M. P. Baldwin, and S. Solomon: Stratosphere–Troposphere Coupling in the Southern Hemisphere. J. Atmos. Sci., 62, 708–715, https://doi.org/10.1175/JAS-3321.1, 2005.

Thompson, D. W. J., & Wallace, J. M.: Annular modes in the extratropical circulation. Part I: Month-to-month variability. Journal of Climate, 13(5), 1000–1016. https://doi.org/10.1175/1520-0442(2000)01360;1000:amitec62;2.0.co;2, 2000.

Tilmes, S., Richter, J. H., Kravitz, B., MacMartin, D. G., Glanville, A. S., Visioni, D., Kinnison, D. E., and Müller, R.: Sensitivity of total column ozone to stratospheric sulfur injection strategies, Geophys. Res. Lett., 48, e2021GL094058, https://doi.org/10.1029/2021GL094058, 2021.

Tilmes, S., Visioni, D., Jones, A., Haywood, J., Séférian, R., Nabat, P., Boucher, O., Bednarz, E. M., and Niemeier, U.: Stratospheric ozone response to sulfate aerosol and solar dimming climate interventions based on the G6 Geoengineering Model Intercomparison Project (GeoMIP) simulations, Atmos. Chem. Phys., 22, 4557–4579, https://doi.org/10.5194/acp-22-4557-2022, 2022.

Walz, R., H. Garny, and T. Birner: Stratospheric Modulation of Tropical Upper-Tropospheric Warming-Induced Circulation Changes in an Idealized General Circulation Model. J. Atmos. Sci., 80, 611–631, https://doi.org/10.1175/JAS-D-21-0232.1, 2023.

Wang, S., E. P. Gerber, and L. M. Polvani: Abrupt circulation responses to tropical upper-tropospheric warming in a relatively simple stratosphere-resolving AGCM. J. Climate, 25, 4097–4115, https://doi.org/10.1175/JCLI-D-11-00166.1, 2012.

Visioni, D., Bednarz, E. M., Lee, W. R., Kravitz, B., Jones, A., Haywood, J. M., and MacMartin, D. G.: Climate response to off-equatorial stratospheric sulfur injections in three Earth system models – Part 1: Experimental protocols and surface changes, Atmos. Chem. Phys., 23, 663–685, https://doi.org/10.5194/acp-23-663-2023, 2023a.

Visioni, D., Bednarz, E. M., MacMartin, D. G., Kravitz, B., Goddard, P.: The choice of baseline period influences the assessments of the outcomes of Stratospheric Aerosol Injection, Earth's Future, 2023b (submitted).

Zhang, Y., MacMartin, D. G., Visioni, D., Bednarz, E., and Kravitz, B.: Introducing a Comprehensive Set of Stratospheric Aerosol Injection Strategies, EGUsphere [preprint], https://doi.org/10.5194/egusphere-2023-117, 2023.

Supplementary Material to:

Potential non-linearity in the high latitude circulation and ozone response to stratospheric aerosol injection

Ewa M. Bednarz[1,2,3], Daniele Visioni[3,4], Amy H. Butler[2], Ben Kravitz[5,6], Douglas G. MacMartin[3], Simone Tilmes[4]

1. Cooperative Institute for Research in Environmental Sciences (CIRES), University of Colorado Boulder, Boulder, CO, USA
2. NOAA Chemical Sciences Laboratory (NOAA CSL), Boulder, CO, USA
3. Sibley School of Mechanical and Aerospace Engineering, Cornell University, Ithaca, NY, USA
4. National Center for Atmospheric Research (NCAR), Atmospheric Chemistry Observations and Modelling (ACOM), Boulder, CO, USA
5. Department of Earth and Atmospheric Sciences, Indiana University, Bloomington, IN, USA
6. Atmospheric Sciences and Global Change Division, Pacific Northwest National Laboratory, Richland, WA, USA

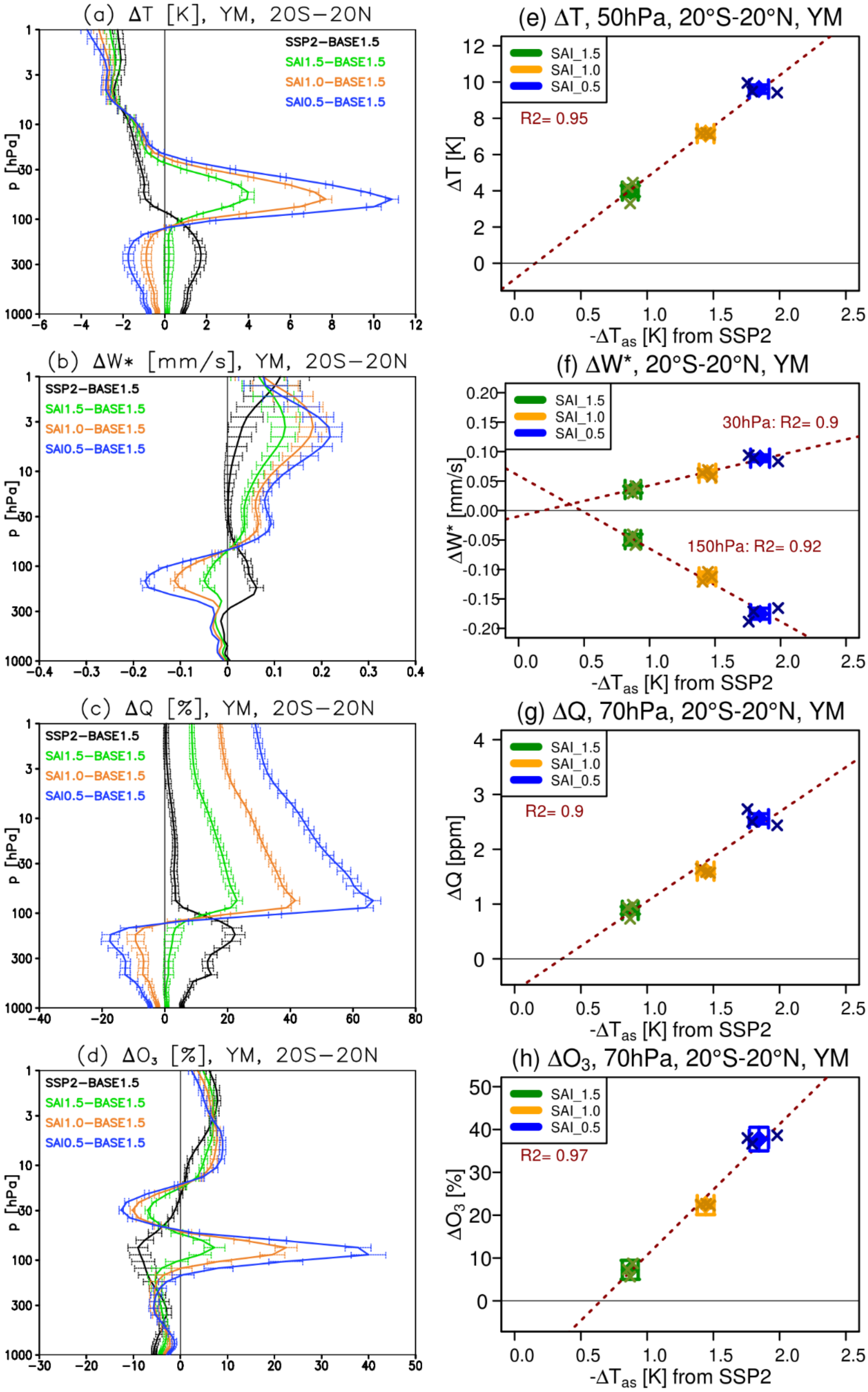

Figure S1. As in **Figure 1** of the main text but for the responses compared to the present day (2020-2039) baseline period BASE1.5.

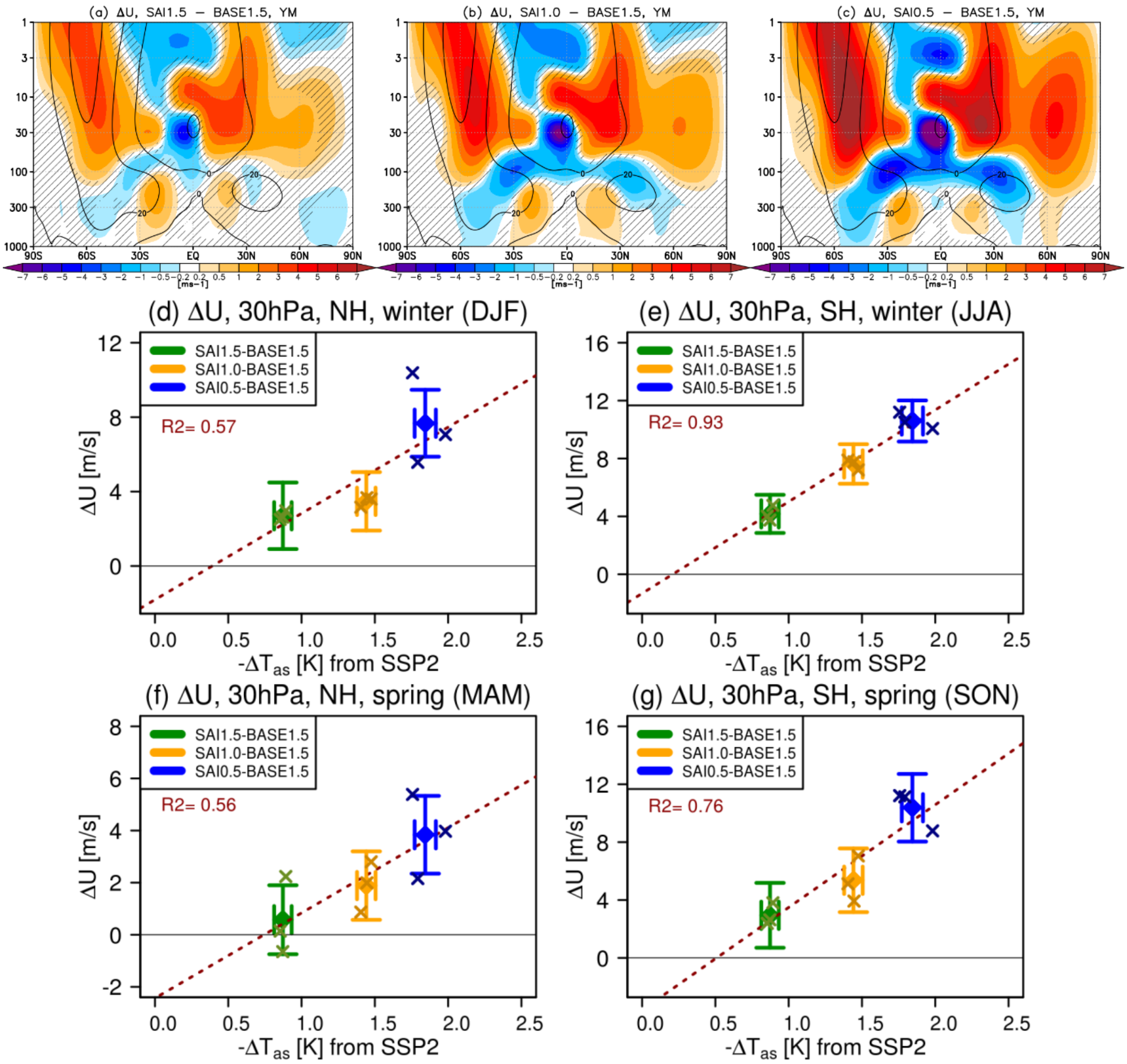

Figure S2. As in **Figure 2** of the main text but for the responses compared to the present day (2020-2039) baseline period BASE1.5

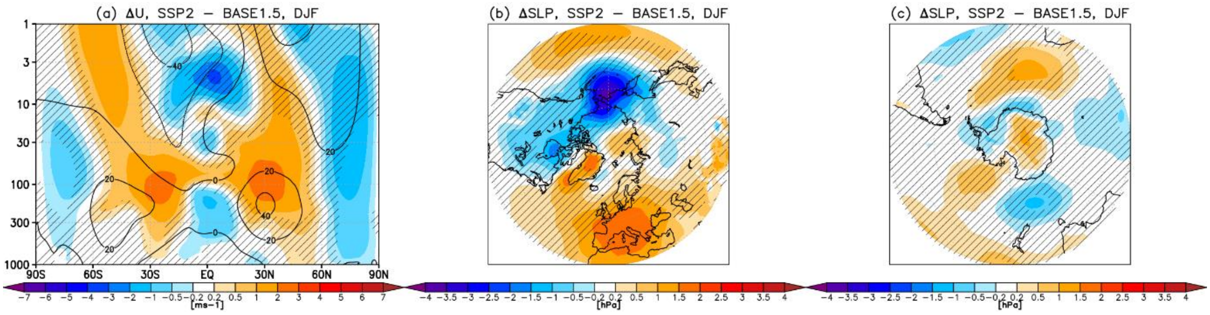

Figure S3. DJF mean changes in (a) zonal wind, (b) sea-level pressure northward from 30N, and (c) sea-level pressure southward of 30S for SSP2-4.5 averaged over 2050-2069 compared to the present day baseline period BASE1.5. Hatching marks the regions where the response is not statistically significant (taken as ±2 standard error of the difference in means).

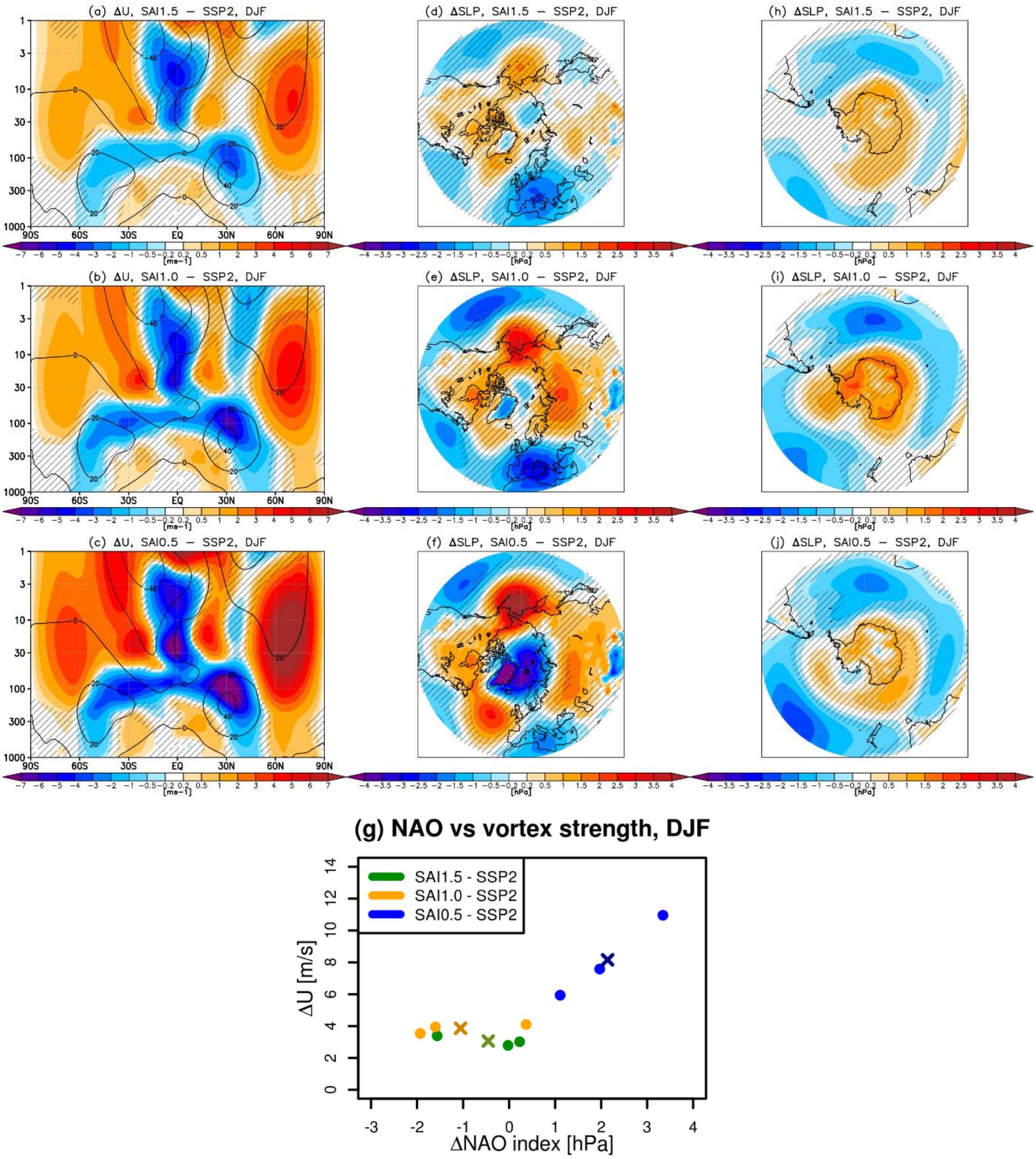

Figure S4. As in **Figure 3** of the main text but for the responses compared to SSP2-4.5.

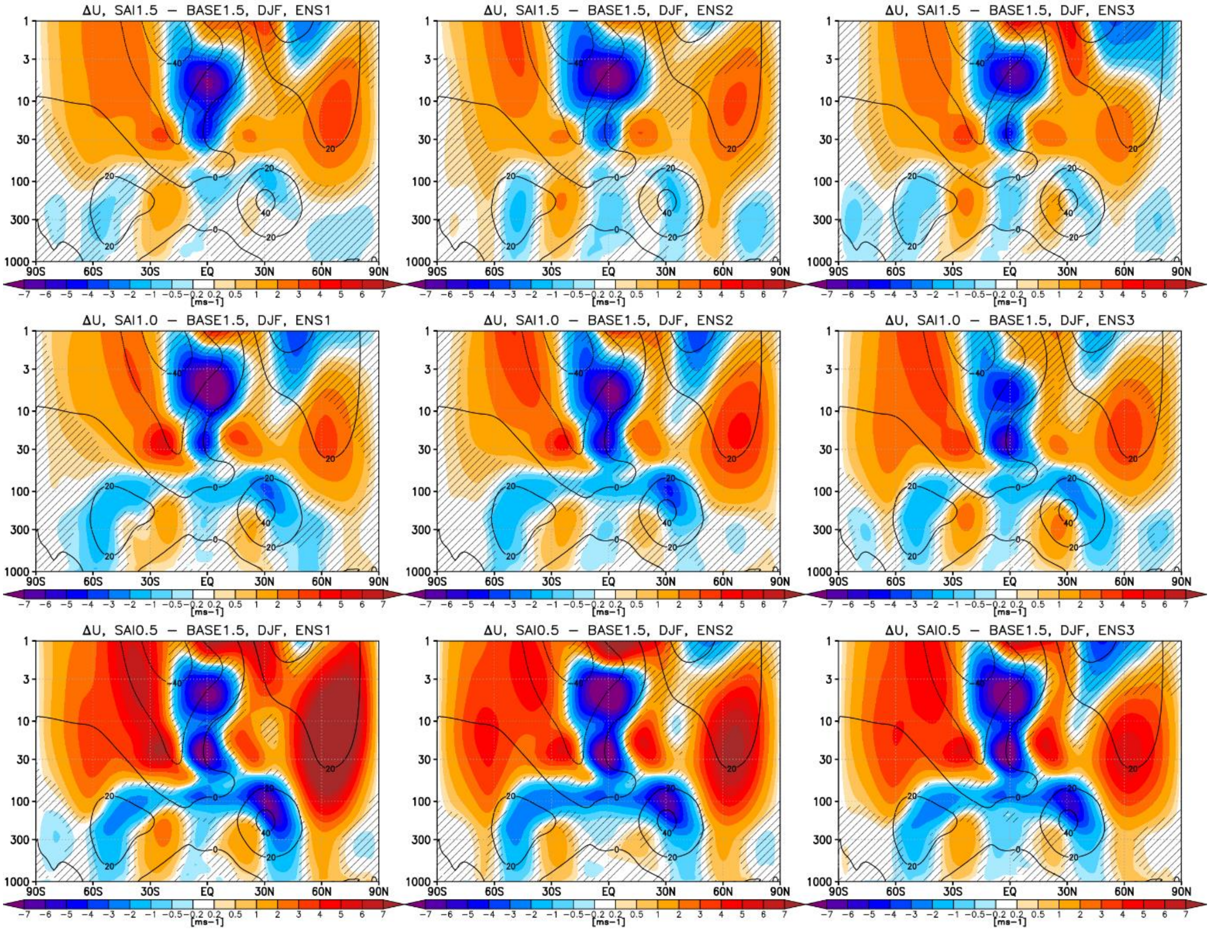

Figure S5. Shading: DJF mean changes in zonal wind simulated in each of the induvial ensemble member (ENS1-ENS3, columns) of the SAI1.5 (top), SAI1.0 (middle) and SAI0.5 (bottom) simulations compared to the ensemble mean of BASE1.5. Contours show the BASE1.5 climatology for reference. Hatching denotes the regions where the response is not statistically significant (±2 standard errors)

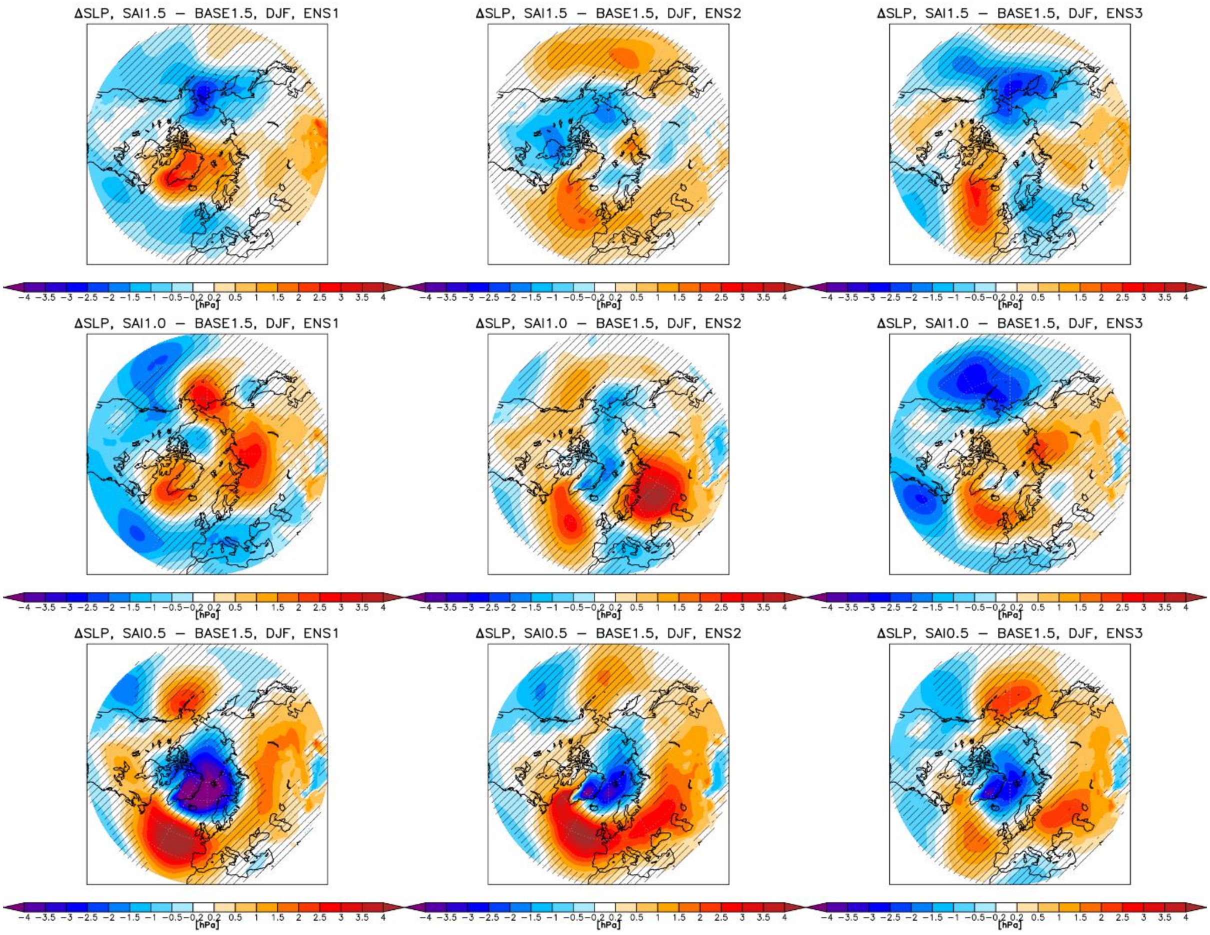

Figure S6. Shading and hatching as in Fig. S5 but for the sea-level pressure response.

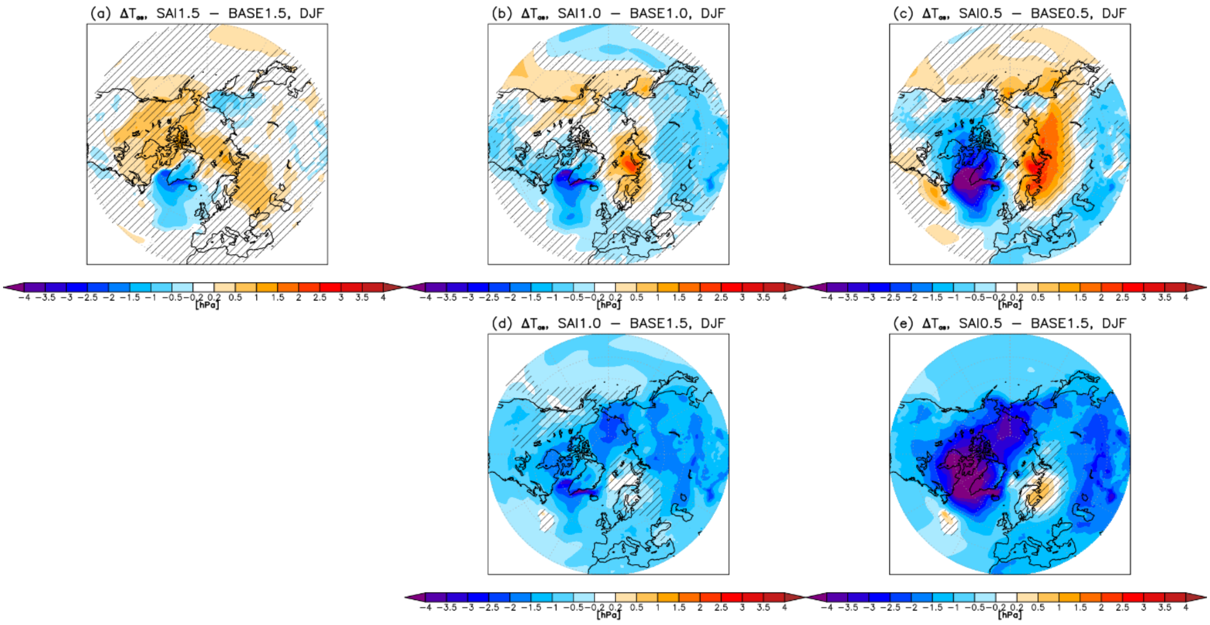

Figure S7. DJF changes in near-surface air temperatures northward of 30°N for each of the SAI scenario (columns) compared to (a-c) each respective baseline period and compared to (a, d-e) the same quasi-present day BASE1.5 baseline period. Hatching as in Fig. 2.

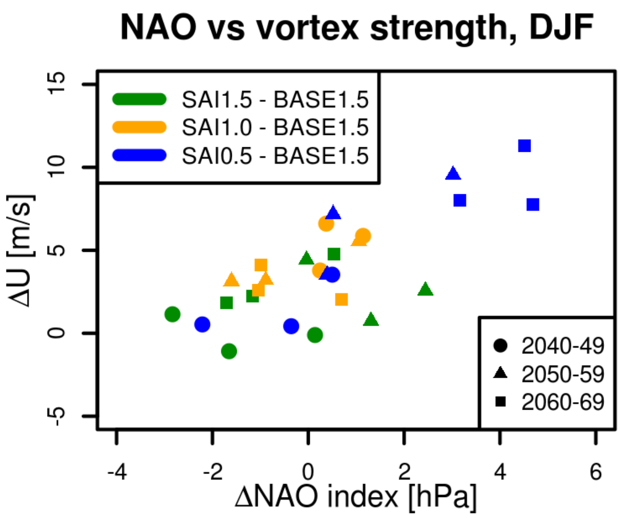

Figure S8. Correlation between the DJF changes in the strength of the NH stratospheric polar vortex (60°N, 30 hPa) and the NAO sea-level pressure index for each of the SAI scenarios and ensemble members, averaged over 10-year-long intervals, compared to BASE1.5.

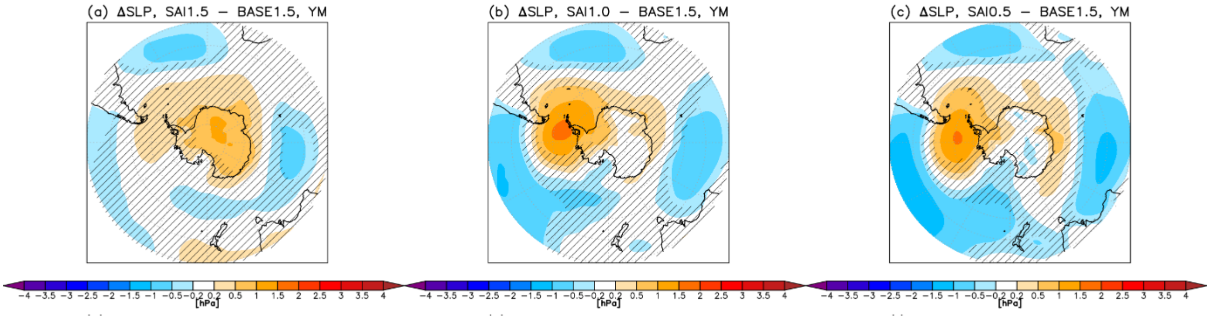

Figure S9. Yearly mean changes in sea-level pressure southward of 30°S for each of the SAI scenario (columns) compared to BASE1.5. hatching as in Fig. 2.